Instabilities and pattern formation in crystal growth*

J. S. Langer

Physics Department and Center for the Joining of Materials, Carnegie-Mellon University, Pittsburgh, Pennsylvania 15213

Several common modes of crystal growth provide particularly simple and elegant examples of spontaneous pattern formation in nature. Phenomena of interest here are those in which an advancing nonfaceted solidification front suffers an instability and subsequently reorganizes itself into a more complex mode of behavior. The purpose of this essay is to examine several such situations and, in doing this, to identify a few new theoretical ideas and a larger number of outstanding problems. The systems studied are those in which solidification is controlled entirely by a single diffusion process, either the flow of latent heat away from a moving interface or the analogous redistribution of chemical constituents. Convective effects are ignored, as are most effects of crystalline anisotropy. The linear theory of the Mullins-Sekerka instability is reviewed for simple planar and spherical cases and also for a special model of directional solidification. These techniques are then extended to the case of a freely growing dendrite, and it is shown how this analysis leads to an understanding of sidebranching and tip-splitting instabilities. A marginal-stability hypothesis is introduced; and it is argued that this intrinsically nonlinear theory, if valid, permits aone to use results of linear-stability analysis to predict dendritic growth rates. The review concludes with a discussion of nonlinear effects in directional solidication. The nonplanar, cellular interfaces which emerge in this situation have much in common with convection patterns in hydrodynamics. The cellular stability problem is discussed briefly, and some preliminary attempts to do calculations in the strongly nonlinear regime are summarized.

CONTENTS

I. INTRODUCTION

Outside the realm of biology, some of the most beautiful and familiar examples of spontaneous pattern formation in nature can be found in the growth of crystals. We all have admired snowflakes; and most physicists are aware of the dendritic—that is, tree-like—microstructures which occur during the solidification of alloys. Solidifying systems are extremely interesting for scientific and technological as well as aesthetic reasons. Compared to complex biological processes, these systems represent conceptually simple examples of self-organization; but we shall see that, even here, the underlying mechanisms are not well understood.

Traditional studies of crystal growth, especially among physicists, have focused primarily on symmetries of atomic arrangements, surface anisotropies, and, more generally, on those near-equilibrium properties which are dominated by atomic and crystallographic effects. The formation of complex solidification patterns, however, is an intrinsically nonequilibrium phenomenon which has been studied, out of necessity, mostly by metallurgists who must deal in a very practical way with these phenomena in the design of materials processes.[1] In this essay, I shall present a physicist's interpretation of some of the previous work on the nonequilibrium problem, and shall supplement this review with a more speculative discussion of recent developments. I shall try to describe the problem in such a way as to emphasize its relationship to a number of apparently similar self-organizing systems that have become fashionable among physicists, chemists, biologists, and mathematicians.

As prelude to a more detailed presentation of special solidification problems, it will be useful to think a bit about the snowflake. Real snowflakes—those that fall from real clouds—are formed by more complicated processes than those which we shall consider here; but they provide a good starting point for posing questions. A typical snowflake, traced from a photograph by Nakaya (1954), is shown in Fig. 1. The pattern is planar and has the hexagonal symmetry characteristic of ice crystals. The snowflake has grown out from a central nucleus; and growth has occurred in a number of stages, each stage being governed by the external conditions encountered by the developing crystal as it is carried through different regions of the atmosphere. The six main dendritic branches of the crystal are essentially, but not precisely, identical to one another.

*Research supported in part by AFOSR Grant F44620-76-C-0103.

[1] I shall make no attempt here to provide a complete review of the metallurgical literature. A good starting point for such a survey is the book *Crystal Growth*, edited by B. R. Pamplin. In particular, see the articles on interfacial stability by Delves (1975) and dendrites by Doherty (1975). A more basic reference is Chalmers (1964).

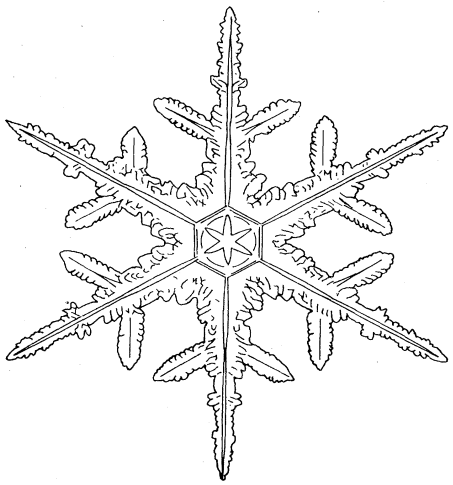

FIG. 1. Snowflake, adapted from a photograph by Nakaya (1954).

There is no internal controlling mechanism which coordinates the growth of these branches, no predetermined set of plans for the construction of this particular snowflake. On the contrary, the growth at any instant must have been controlled only by a simple set of spatially uniform external conditions—the temperature and the humidity and, perhaps, the concentrations of various air pollutants. These slowly varying quantities have determined nearly identical growth patterns along each of the branches.

The snowflake brings to mind some of the most basic questions in the problem of pattern formation. How do patterns emerge from a structureless environment? Why, under some circumstances, does nature make snowflakes instead of, say, simple shapes such as discs or hexagonal plates or, at the opposite extreme, disordered structures? Why are the patterns so very sensitive to growth conditions and material parameters? Minute changes in temperature and humidity cause qualitative changes in growth patterns; thus, no two snowflakes seem to be alike. As we shall see, crystalline anisotropy may be a relatively weak effect; yet it accurately controls the symmetry of dendritic structures. How can we account for this special sensitivity?

Several steps toward answers to the first of these questions are understood in some detail. We know that substances in which the molecules are tightly bound on crystallographic planes will form regularly faceted solids under wide ranges of growth conditions. A great deal of progress has been made in understanding the energetics of facet-formation (Jackson *et al.*, 1967) and in modeling mechanisms for the slow growth that occurs on molecularly smooth crystalline surfaces (see reviews by Muller-Krumbhaar, 1978; Weeks and Gilmer, 1979). Our emphasis, however, will be on the opposite situation. We shall consider only those substances for which molecular binding at the surface is sufficiently weak that growth is rapid and is controlled solely by the diffusion fields in the neighborhood of the solidification front. For such substances, the fluid-solid interfaces are rough at the molecular level but smoothly rounded on a macroscopic scale. Substances in this latter category include most metals and alloys and some organic crystals that have been specially useful for experimental purposes. Ice, as it turns out, is an intermediate case in which slowly growing facets occur parallel to the basal plane but surfaces are rounded and growth is rapid in the hexagonal directions.

The other part of the solidification problem in which significant progress has been made has to do with the stability of simple growth forms. Given diffusion control, as opposed to interface control of the solidification process, we shall see that simple shapes such as planes, spheres, cylinders, etc., are unstable under certain commonly encountered growth conditions. Roughly speaking, this instability occurs because diffusion kinetics favors configurations in which the growing solid has as large a surface area as possible. Latent heat, for example, is dissipated more rapidly in such configurations. Ultimately, this morphological instability of the solidification front is limited by capillary forces; and it is the interplay between capillary and kinetic effects which somehow produces the complex growth patterns that we see in nature.

The big, unsolved part of the problem is how these complex shapes are selected. In only one case, that of the free dendrite, do we seem to have found a clue to a special selection principle; and the evidence to date indicates that this particular mechanism is more subtle than had previously been suspected. Superficially, however, this close connection between instabilities and pattern formation seems to fit the general scheme that is emerging in related areas of investigation. We shall see that there is a striking similarity between the planar instability that leads to cellular solidification fronts and the Bénard instability that produces convection cells in a fluid[2]; and, in addition, there are analogous theoretical difficulties in predicting the features of these dynamically restabilized systems. More analogs are found in chemically reacting systems (Liesegang rings, Zhabotinsky reactions, etc.), in lasers, in superconducting devices, and even in classical nonlinear systems such as musical instruments.

The phenomenological picture looks seductively general. In each of the above examples, an initially quiescent system becomes unstable at a critical value of some control parameter—the temperature gradient, the composition, the pump-rate—and then restabilizes into a more complex, space- or time-dependent configuration. As the control parameter is increased further, the system may undergo additional transitions into more complex states or into states which are intrinsically chaotic. The hydrodynamic system may become turbulent; the musical instrument may produce noise. The apparent universality of this class of phenomena has inspired a number of important attempts to construct a unified theoretical framework for their analysis. Most prominent among these theoretical programs are Thom's catastrophe theory (Thom, 1975), Prigogine's concept of dissipative structures (Glans-

[2]The basic reference for the convective instabilities is Chandrasekhar (1961). For a more recent review of both the experimental and theoretical situations, see Whitehead (1975).

dorff and Prigogine, 1971; Nicolis and Prigogine, 1977), and Haken's synergetics (Haken, 1977). Each of these formalisms has had notable success in the description of systems where the number of relevant degrees of freedom is small, as in the few-mode laser or the spatially homogeneous chemical reaction.

My own opinion, which motivates much of what is said in this essay, is that neither the breadth nor the depth of the conjectured universality principle are well established, and that what is needed now is not further generalization but detailed analysis of experimentally realizable, physical systems. In the solidification problem, there emerge rich mathematical structures which are specific to particular models, which do not seem to have analogs in, say, the nonlinear theory of homogeneous chemical reactions, but which appear to be absolutely essential for the understanding of particular modes of crystal growth. Perhaps, when we understand these mechanisms more completely, we shall see that they fit neatly into the formal schemes that have been proposed. My intention is not to cast doubt on the validity of any of these schemes, but simply to argue that the appropriate next phase of research in this area should consist of a large amount of open-minded spadework.

With this bias in mind, I have organized the main sections of this paper as follows. Section II contains qualitative descriptions of several selected classes of solidification processes and brief mathematical statements of what are believed to be the simplest physical models capable of exhibiting the observed phenomena. Section III is devoted to linear stability analyses of the quiescent, planar and spherical, steady-state solutions of these models. Thus Secs. II and III constitute, for the solidification problem, a selective review of the first part of the pattern-formation analysis—the identification of the initial instabilities. In the following two sections, we shall look at the restabilization problem, first for free dendrites in Sec. IV, and finally for periodic cellular structures in Sec. V.

II. PHENOMENA AND MODELS

A. Solidification of a pure liquid

The simplest situation of interest to us is the solidification of a pure substance from its melt, for example, the freezing of ice in a sample of pure water. (The reverse process, melting, can be equally interesting; and all of the phenomena described below have reverse analogs. For clarity, however, it will be easiest to think primarily about solidification.) In the case of a pure substance, the process is governed entirely by heat flow. That is, the rate of solidification at any point along the liquid-solid interface is governed by how rapidly the latent heat generated (or absorbed) at that point can be conducted into the bulk of the sample or removed at the boundaries.

Consider, now, the two related experimental arrangements illustrated schematically in Fig. 2. In both cases, a pure fluid is contained in a vessel whose walls are held at some temperature T_W which is less than the melting temperature T_M; thus heat is extracted through the walls. In the first case (a), the liquid is initially at

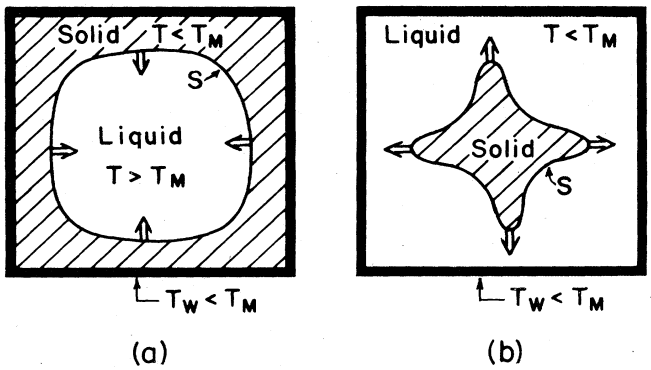

FIG. 2. Schematic illustration of solidification occurring in (a) stable and (b) unstable configurations.

a temperature $T \geq T_M$, and the solid is allowed to start forming at the walls. As we shall see, this situation is completely stable. The solidification front S moves smoothly and uniformly in toward the center, its motion being determined by the rate at which the excess heat energy of the solidifying fluid can be conducted out through the surrounding solid. The second case (b) is more interesting. Here, the liquid is initially undercooled to a temperature $T < T_M$, and solidification is initiated at a seed crystal at the center of the vessel. The latent heat generated at the interface S must be conducted through the liquid in order for the crystal to grow. If one is careful, convective heat transport can be eliminated, so that the problem remains one of thermal diffusion. This situation is intrinsically unstable; the interface S breaks up into dendrites which grow relatively rapidly out from the central seed. The crucial difference between the stable case (a) and the unstable case (b) is that, in (b), the solidification front advances into a metastable phase, that is, into an undercooled melt.

Real snowflakes are formed under conditions which are roughly analogous to case (b); they grow out from seeds in an environment of supersaturated water vapor. Of course, growth is much slower in the atmosphere because the density of water molecules in the vapor is very much less than that in liquid. Another difference is that there is air present to transport heat. These differences seem to be of only second-order importance, however. The experimental arrangement of case (b) is capable of producing dendritic crystals under conditions which can be carefully controlled and which are convenient for theoretical analysis.

The most complete experiments of this kind have been carried out by Glicksman, Schaefer, and Ayers (1976) who used succinonitrile as a working substance. Similar experiments using ice have been performed by Fujioka (Fujioka, 1978; Sekerka, 1976; Langer *et al.*, 1978). To illustrate the technique, I have reproduced one of Fujioka's artificial snowflakes in Fig. 3. The crystal has been seeded inside a uniformly supercooled sample of fluid by allowing the solid phase to grow through a vertical capillary tube and to emerge through an orifice at the center of the container. Subsequent growth of the crystal has been observed photographically. The most interesting quantities to measure are

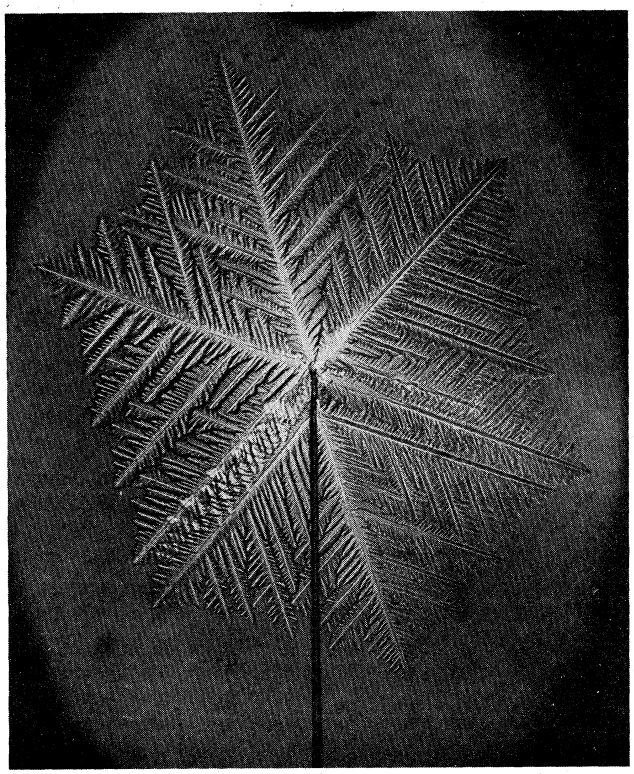

FIG. 3. Photograph of dendritic ice crystal grown in pure water at an undercooling of $T_M - T = 2.34°C$ (Fujioka, 1978).

the growth velocities and shapes of the frontmost tips of primary dendrites, and the spacings of emerging sidebranches. These quantities turn out to be accurately reproducible as functions of the initial degree of undercooling of the fluid, which is the single control parameter in this system. We shall return to this version of the solidification problem, with special emphasis on the succinonitrile experiments, when we discuss the theory of dendritic growth in Sec. IV.

The mathematical problem of predicting the motion of the solidification front in the above examples may loosely be described as a Stefan problem (Rubinstein, 1971), although there are several important differences between the version of this problem which is of interest to us and the way the problem usually is understood by mathematicians. The basic ingredient is a diffusion field, in this case the temperature T, which satisfies an equation of the form:

$$D_T \nabla^2 T = \partial T/\partial t , \tag{2.1}$$

where D_T is the thermal diffusion constant. In general, we must write (2.1) separately for the liquid and solid phases, which usually will have different values of D_T. In the following, we shall use primed symbols to denote properties of the solid, and shall let unprimed symbols refer to the liquid. Thus the diffusion equation for the solid is the same as (2.1) but with D_T replaced by D_T'. The condition of heat conservation at a point on the moving interface takes the form:

$$L v_n = [D_T' c_p' (\nabla T)_{\text{Solid}} - D_T c_p (\nabla T)_{\text{Liquid}}] \cdot \hat{n} , \tag{2.2}$$

where the left-hand side is the rate at which heat is generated at the boundary, and the right-hand side is the rate at which this heat flows into the bulk phases on either side. Here, L is the latent heat per unit volume of the solid; c_p and c_p' are the specific heats per unit volume of the liquid and solid, respectively; v_n is the normal velocity of the interface; and $\hat{n}$ is the unit normal at the interface, directed into the liquid. The gradients are evaluated at the interface in the indicated phases. In order to preserve a purely diffusive model, we shall ignore any density difference between liquid and solid phases.

To complete the specification of this model, we must introduce a thermodynamic boundary condition at the interface. The simplest choice would be to say that the temperature must be exactly the bulk melting temperature along the surface of instantaneous two-phase coexistence; and, if we do this, we recover something which is, in principle, very much like the Stefan problem as it occurs in the mathematical literature. Unfortunately, this relatively tractable mathematical version of the problem omits the effect of surface tension, which provides the crucial stabilizing force necessary for pattern formation. The correct form of the thermodynamic boundary condition is

$$T(\text{Interface}) = T_M [1 - (\gamma \mathcal{K}/L)] , \tag{2.3}$$

where γ is the liquid-solid surface tension, and $\mathcal{K}$ is the curvature of the interface, here understood to be positive if the center of curvature lies on the solid side of the interface, that is, if the solid bulges into the liquid. Equation (2.3) is a form of the Gibbs–Thomson relation (see Turnbull, 1956) which predicts, among many other things, a reduction of the melting temperature for small particles, and a finite activation energy for homogeneous nucleation of a solid in an undercooled liquid. Note that the ratio γ/L has the dimensions of a length. It turns out that, without this length or something else to replace it, the conventional Stefan problem cannot conceivably describe pattern formation of the kind seen in nature; it lacks the dimensional information needed to set the scale of a pattern.

Equations (2.1), (2.2), and (2.3) completely specify the model of solidification of a pure substance which we shall adopt for study later in this paper. Before going on to the description of other models, however, a few remarks about mathematical and metallurgical points of view may be useful.

As has been indicated already, the free-boundary problem posed above appears to be much more ferocious than the Stefan problem as conventionally posed by mathematicians. Not only do we need a more difficult boundary condition in (2.3), but we insist on dealing with complex surfaces in three dimensions instead of the effectively one-dimensional situations most often considered in mathematical studies. We do have a few compensating advantages, however, in that we do not ask for really general solutions of the problem. We never need to concern ourselves with externally imposed space- or time-dependent temperature distributions at the walls of our systems; and, most often, we

shall be able to replace these walls by simple boundary conditions at infinity. Moreover, we are permitted occasionally to use some cautious physical intuition in place of rigorous mathematics in order to assure ourselves that problems are well posed and that solutions exist.

While the free-boundary problem posed here may seem impossibly complicated to a mathematician, it still appears to be naively oversimplified to a metallurgist. We are omitting convection in the fluid and are ignoring a number of potentially crucial effects caused by impurities or other defects in the system. Most important, we are assuming that all interfaces are molecularly rough (i.e., not faceted), and that we can neglect all effects of crystalline anisotropy. One of the most striking characteristics of the snowflakes in Figs. 1 and 3 is their hexagonal symmetry; yet this symmetry seems nowhere to be included in the proposed model. In principle, we should include an orientation dependence in the surface tension γ, and also should allow for anisotropic heat flow in the solid. Another potentially important crystalline anisotropy occurs in the molecular attachment kinetics, an effect which we have omitted entirely so far. To see what this effect is, note that the thermodynamic boundary condition (2.3) is a local-equilibrium approximation. Strictly speaking, it applies only to a stationary interface in thermal equilibrium with its surroundings. In a non-equilibrium situation where the interface is moving, a finite discontinuity in the chemical potential across the interfacial region may be necessary to drive liquid molecules onto the solid surface. This effect is usually assumed to show up as an additional anisotropic term proportional to some power of the growth velocity v_n on the right-hand side of (2.3) (see Tarshis and Tiller, 1967). For example, such a term can reflect the fact that ice crystals grow only very slowly in a direction perpendicular to the basal plane, and thus snowflakes turn out to be flat, feathery structures (see Hobbs, 1974).

Despite these valid objections, we shall continue to work with the isotropic, local-equilibrium version of this model. As it stands, this model exhibits a rich variety of instabilities and self-organizing processes. With only a modest supplement to account for crystalline anisotropy, the model even seems to provide a quantitatively accurate explanation of dendritic growth rates.

B. Isothermal solidification of a liquid mixture

Alert readers may have been puzzled by the statement, some paragraphs ago, that the solidification process illustrated in Fig. 2(a) is intrinsically stable. This process looks much like the quenching of an ingot of molten metal; and such quenched specimens usually exhibit extremely irregular solidification patterns. The difference is that metallurgical materials are seldom, if ever, pure substances. In alloys—even those which are very dilute—the diffusion of chemical species may control the motion of a solidification front in a manner exactly analogous to the way the motion is governed by thermal diffusion in the case of a pure substance. Because thermal diffusion is always very much faster than chemical diffusion (especially in a metal), temperature deviations must relax in times which are much shorter than the time required for rearrangement of chemical species; thus solidification is effectively isothermal and chemical effects are dominant. In the quenched ingot, it is chemical kinetics which causes interfacial instabilities.

To see the analogy between the thermal and chemical cases, consider a typical phase diagram of a binary alloy, a portion of which is illustrated schematically in Fig. 4. Here, C denotes the concentration of what we shall call the solute, and T_0 is the local temperature which, for present purposes, we shall assume to be constant over a large region of the sample. In two-phase equilibrium, the solute concentration in the liquid is appreciably greater than in the solid; that is, C_{eq} is greater than C'_{eq}. Thus an advancing solidification front rejects solute molecules in much the same way as, in the pure thermal case, it releases latent heat; and the rate at which the excess solute can be transported away from the interface governs how rapidly the interface can move.

The analogy to the thermal case becomes particularly clear if one writes the equations of motion in terms of chemical potentials instead of concentrations. Let μ be the chemical potential of solute molecules relative to that of solvent,[3] and let $\tilde{\mu}$ be the difference between μ and its equilibrium value for two-phase coexistence at T_0

$$\tilde{\mu} \equiv \mu - \mu_{eq}(T_0) \,. \tag{2.4}$$

If the deviations from equilibrium are small, we have relations of the form

$$\tilde{\mu}(\text{Liquid}) = \left(\frac{\partial \mu}{\partial C}\right)\Big|_{C=C_{eq}} \delta C; \quad \tilde{\mu}(\text{Solid}) = \left(\frac{\partial \mu}{\partial C}\right)'\Big|_{C=C'_{eq}} \delta C' ; \tag{2.5}$$

where the δC's are the local concentration deviations. Then the diffusion equation in the liquid can be written

$$D_C \nabla^2 \tilde{\mu} = \partial \tilde{\mu}/\partial t \,, \tag{2.6}$$

where D_C denotes the chemical diffusivity; and there

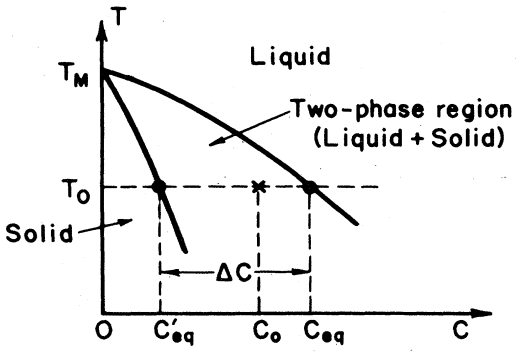

FIG. 4. Portion of the phase diagram of a binary solution.

[3]For simplicity, we specialize to the case in which the partial molar volumes are the same for all species and do not vary from phase to phase.

will be a similar equation with D_C' denoting the corresponding diffusivity for the solid. For simple systems of this kind, it is conventional to write the diffusivity in the form

$$D_C = M(\partial\mu/\partial C)\,, \tag{2.7}$$

where M is proportional to a mobility. Then the continuity equation analogous to (2.2) becomes

$$v_n \Delta C = [M'(\nabla\tilde{\mu})_{\text{Solid}} - M(\nabla\tilde{\mu})_{\text{Liquid}}]\cdot\hat{n}\,, \tag{2.8}$$

where ΔC is the miscibility gap shown in Fig. 4. [Strictly speaking, the ΔC appearing in (2.8) should be modified by curvature effects; but that correction turns out to be negligible under ordinary circumstances.] Finally—and this is the main advantage of the chemical-potential notation—the condition of local equilibrium at the interface is simply that $\tilde{\mu}$ be continuous there and that it have the value

$$\tilde{\mu}(\text{Interface}) = -(\gamma/\Delta C)\mathcal{K} \tag{2.9}$$

where γ and $\mathcal{K}$ are surface tension and curvature as defined following (2.3).

What, then, happens in the quenched ingot? Suppose that the quench is spatially uniform, so that the system finds itself initially everywhere at T_0 in the liquid phase. Of course, the initial concentration, say C_0, must be less than C_{eq}, or else no solidification will take place. A plausible assumption is that the initial quench takes the system to a temperature T_0 which is just low enough that C_0 is slightly less than C_{eq}; that is, the liquid in the bulk of the container is at the point in the phase diagram indicated by the X in Fig. 4. This liquid is effectively supercooled [the metallurgical term is "constitutionally supercooled" (Tiller *et al.*, 1953)]; and the solidification front which starts moving in from the walls toward the center is unstable. Under the conditions described here, a forest of solute-poor dentrites ($C = C_{eq}'$) will grow inward from all sides, filling the container, and leaving solute-rich fluid in the interstices which, at this temperature, constitute most of the volume. If the temperature is subsequently reduced, the interstitial fluid will solidify; but evidence of the dendrites will remain in the solute-segregation pattern. Moreover, because each dendritic branch retains the crystalline orientation of the primary stem from which it arose, each individual dendritic structure plus its associated solid interstices forms a coherent crystal, that is, a grain. Thus the dendritic mechanism determines both the chemical microstructure (usually on a scale of microns) and the larger-scale grain structure of the quenched alloy.

C. Directional solidification

The third and final kind of model that I should like to introduce is one which is relevant to processes like directional solidification or zone refinement of multicomponent materials. As in the last example, the dominant kinetic effect will be chemical diffusion; but here we shall impose an additional temperature gradient to control the orientation and velocity of the solidification front. With this extra degree of control, the system can be made to undergo one or more of the classic—i.e., Bénard-like—pattern-forming transitions.

The basic features of the system are shown in Fig. 5. The sample consists of a long rod or a long thin strip of the working material which is drawn, at a predetermined velocity v, through a fixed temperature gradient established by stationary hot and cold contacts at A and B, respectively. The temperatures at A and B are supposed to be chosen so that the sample is molten at A and solid at B, and so that the interface is visible in between.

Strictly speaking, this system is one in which both the thermal and chemical diffusion fields are nontrivially coupled to one another. As long as the thermal diffusion constant is much larger than the chemical diffusivity, however, and as long as the latent heat is not too big, we may ignore the heat generated at the interface. Then, without much additional loss of generality, we may assume that the thermal conductivities are about the same in both liquid and solid phases, and write simply that the temperature throughout the active region (A–B) is

$$T = T_0 + Gz\,. \tag{2.10}$$

Here, z is the position coordinate shown in Fig. 5; T_0 is some reference temperature to be chosen shortly; and G is the impressed temperature gradient. [The problem of the coupling between thermal and chemical effects has been examined in much more detail by Wollkind and Segel (1970), to whom we shall refer in Sec. V.]

We are already in a position to understand much of what happens in this system. Let us suppose that the sample is long enough and that the interface is stable enough that we can achieve steady-state motion with the given v and G. Now consider the phase diagram in Fig. 6. Because of Eq. (2.10), the T axis in this figure is effectively a z axis, and we can draw the composition profile $C(z)$ directly on the diagram. This is the heavy dashed line, shown here for the case of a flat interface at temperature T_0, that is, at $z = 0$. Note that

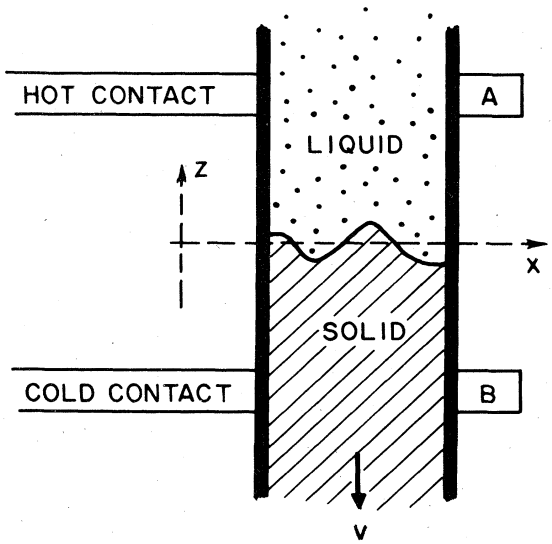

FIG. 5. Schematic arrangement of a directional-solidification experiment.

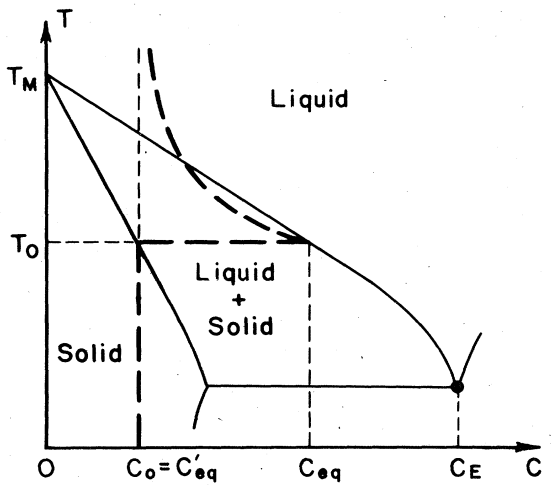

FIG. 6. Portion of the phase diagram of a binary solution. The heavy dashed line indicates the composition profile in the neighborhood of a flat interface for a system undergoing directional solidification as described in the text.

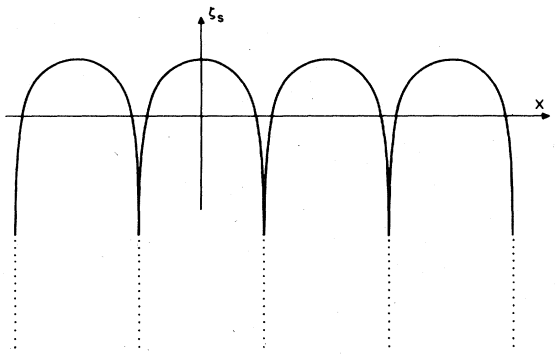

FIG. 7. Cellular interface of the kind seen by Jackson (1971) in directionally solidifying thin samples of CBr_4. The solidification front is moving in the positive-z (upward) direction.

the steady-state condition requires that all of the solute in the liquid be absorbed by the solid; thus $C = C_0$ at infinity on both sides of the interface. The intersection of the vertical line, $C = C_0$, with the solidus determines the temperature T_0 and, therefore, the position of the interface. From here on, we shall adopt this definition of the reference temperature T_0, even for situations where the planar interface is a completely unstable steady-state solution of the problem.

The dashed line in Fig. 6 also illustrates the "spike" in solute concentration which must build up in front of the advancing interface. The concentration gradient in this region must be just large enough to drive the rejected solute forward into the liquid at the velocity v. As v increases, this gradient increases, and, as is shown in the figure, the concentration profile enters the two-phase region. Thus, with increasing v (or decreasing G), we encounter constitutional supercooling and the possibility of an unstable interface. I want to be careful not to overemphasize this point lest I seem to imply that we are dealing with a purely thermodynamic rather than a kinetic instability. We shall see in the next section that the interface in this model does become unstable at a critical value of the ratio v/G, but that this critical value depends on the diffusion coefficients in both the solid and the liquid, and that the underlying mechanism is truly kinetic in nature.

This instability is particularly interesting because apparently, under some conditions, the interface restabilizes into a periodic cellular pattern. Again, I want to insert a word of caution. The conditions under which this theoretical model is known to produce a stable cellular interface are not precisely the same as those for which cellular interfaces have been observed experimentally. We shall review the theoretical situation in Sec. V. For the present, let us assume that the model described here contains all the essential ingredients, and go on now to look at a few experimental observations.

One particularly elegant set of observations has been made by Jackson (1971, film), who looked at a thin sample of C Br_4 contained between two microscope slides and passed at constant velocity across a pair of hot and cold plates exactly as shown in Fig. 5. Stability was most conveniently controlled in this case by successively adding small amounts of impurity rather than by increasing the velocity. The system was seen to undergo two transitions, first from a flat interface to a cellular one, and, second, from cellular to dendritic. A typical cellular pattern of the kind seen by Jackson is drawn in Fig. 7. The structure appears to be nearly stationary in the interface frame of reference, that is, in the frame defined by the coordinates x,z in Fig. 5. Note the asymmetry of this pattern: the warmer leading edges are round and smooth, whereas the cooler trailing grooves are very sharp. The impurity is absorbed almost entirely in these grooves; thus the scalloped interface leaves behind it a solute segregation pattern consisting of parallel lines of impurity-rich material running the length of the sample. Closer inspection of Jackson's photographs, or direct observation of the cells through a microscope, reveals that the steady-state picture may break down in the grooves. It appears that the impurities may be deposited as a series of droplets, the action of the groove-root looking like that of a leaky faucet. If this is always true, then the restabilization mechanism is significantly more interesting than one might have expected.

As simple as these experiments may seem, they have not yet been carried out accurately enough to answer some of the most crucial questions. It is not known for sure whether the cellular and dendritic transitions are really sharp and reproducible. It would be especially interesting to know whether these transitions are hysteretic, that is, whether the critical velocity is the same for both acceleration and deceleration (see Verhoeven and Gibson, 1972). So far as I know, nobody has looked carefully at how the sizes and shapes of the cells evolve as one varies the growth parameters past the threshold of instability. Such measurements have yielded extremely interesting information about the onset of convection patterns in hydrodynamic systems.

Cellular solidification patterns are known to occur in a wide variety of metallurgically important situations.

During solidification of a dilute alloy, an initially flat interface may develop an hexagonal pattern of bulges and depressions which looks very similar to the classic pictures of Bénard convection (Tiller, 1961; Morris and Winegard, 1969). Hexagonal solute segregation patterns are sometimes observed in directionally solidified semiconductor crystals. Related phenomena are known to occur in the formation of aligned eutectics (Jackson and Hunt, 1966). The process of interest in the latter case involves directional solidification of a eutectic alloy near the concentration C_E shown in the phase diagram, Fig. 6. Under stable conditions, the eutectic solid consists of a solvent-rich matrix in which is imbedded a finely spaced array of solute-rich rods or plates aligned parallel to the direction of solidification. At off-eutectic compositions, say $C < C_E$, and at large enough growth velocities, the periodic liquid–eutectic interface itself may become unstable; and a widely spaced pattern of parallel, solvent-rich rods or dendritic structures may emerge within the eutectic solid (Verhoeven and Gibson, 1973). These situations are intrinsically more complicated than anything we have considered so far because they involve three-phase equilibrium; but they are extremely important technologically. Many common alloy phases are really eutectics, e.g., pearlite in steel; and directionally solidified eutectics can have remarkable mechanical or electrical properties. It would be extremely interesting to understand the principle which governs the formation of these structures.

Let us conclude this section by writing down the detailed equations of motion for the two-phase model of directional solidification. These equations are straightforward extensions of our earlier cases. If we want to retain our description of the diffusion field in terms of the chemical potential, we must subtract the variation of μ associated with the temperature gradient. That is, we must write:

$$\left.\begin{aligned}\tilde{\mu}(\text{Liquid}) &\equiv \mu - \mu_{eq}(T_0) - \left(\frac{\partial\mu}{\partial T}\right)\Big|_{T=T_0} Gz \cong \left(\frac{\partial\mu}{\partial C}\right)\Big|_{C=C_{eq}} \delta C \\ \tilde{\mu}(\text{Solid}) &\equiv \mu - \mu_{eq}(T_0) - \left(\frac{\partial\mu}{\partial T}\right)'\Big|_{T=T_0} Gz \cong \left(\frac{\partial\mu}{\partial C}\right)'\Big|_{C=C'_{eq}} \delta C\end{aligned}\right\}. \tag{2.11}$$

Then the diffusion equation in the liquid has the form

$$D_C\nabla^2\tilde{\mu} + v\frac{\partial\tilde{\mu}}{\partial z} = \frac{\partial\tilde{\mu}}{\partial t}; \tag{2.12}$$

and, as before, we must replace D_C by D'_C for the solid. Note that we have allowed for the fact that our coordinate system is moving with velocity v in the z direction with respect to the material in the sample. The continuity equation is essentially unchanged from (2.8), except that we can write a more specific form for the left-hand side. Let the interface occur at a position

$$z(\text{Interface}) = \zeta(\mathbf{x},t), \tag{2.13}$$

where $\mathbf{x}$ is the two-dimensional coordinate shown in Fig. 5. Then we have

$$\Delta C\left(v + \frac{\partial\zeta}{\partial t}\right)(\hat{n}\cdot\hat{z}) = [M'(\nabla\tilde{\mu})_{\text{Solid}} - M(\nabla\tilde{\mu})_{\text{Liquid}}]\cdot\hat{n}, \tag{2.14}$$

where $\hat{z}$ is the unit vector in the z direction. Finally, the thermodynamic (Gibbs–Thomson) boundary condition is

$$\mu - \mu_{eq}(T) = -(\gamma/\Delta C)\mathcal{K}; \tag{2.15}$$

and here it is T rather than T_0 which appears as the argument of μ_{eq}. Assuming that first-order differential approximations are adequate, we can expand (2.15) about T_0 and use the result to evaluate (2.11) at the interface. We find

$$\left.\begin{aligned}\tilde{\mu}(\text{Liquid Interface}) &= -\left(\frac{\gamma}{\Delta C}\right)\mathcal{K} - \left(\frac{\partial\mu}{\partial C}\right)\Big|_{C=C_{eq}}\left|\frac{dC_{eq}}{dT}\right| G\zeta \\ \tilde{\mu}(\text{Solid Interface}) &= -\left(\frac{\gamma}{\Delta C}\right)\mathcal{K} - \left(\frac{\partial\mu}{\partial C}\right)'\Big|_{C=C'_{eq}}\left|\frac{dC'_{eq}}{dT}\right| G\zeta\end{aligned}\right\} \tag{2.16}$$

where the quantities $|dC_{eq}/dT|$ and $|dC'_{eq}/dT|$ are the slopes of the liquidus and solidus respectively.

III. THE MULLINS-SEKERKA INSTABILITY

A. Pure substance: planar interface

In this section, we are going to examine several simple cases of the interfacial instability which drives the pattern-forming process in solidification. Our understanding of this mechanism is due largely to Mullins and Sekerka (1963, 1964; see also Sekerka, 1973) who were the first to perform systematic linear-stability analyses and to point out the underlying kinetic nature of the process.

As so often happens, it is the simplest possible example which provides us with the most physical insight. Accordingly, let us start with either the pure thermal or pure chemical model described above, and consider a flat solidification front advancing with velocity v into an undercooled melt. This is formally the same as the model of directional solidification, but without the stabilizing thermal gradient. I shall emphasize the equivalence of the thermal and chemical models by introducing a dimensionless diffusion field u:

$$u = \begin{cases}\dfrac{T - T_M}{(L/c_p)} \text{ (Thermal model)}; \\ \dfrac{\tilde{\mu}}{\Delta C(\partial\mu/\partial C)} \text{ (Chemical model)}.\end{cases} \tag{3.1}$$

Note that (3.1) has been written using the unprimed liquid-phase parameters c_p and $(\partial\mu/\partial C)$. This one-sided convection seems simplest, but will cause an artificial asymmetry in some of the following formulas. Note also that, in order to preserve the exact equivalence between the two models, we are neglecting the curvature dependence of the miscibility gap ΔC. We shall account for this dependence in the more detailed discussions of directional solidification to be presented in Secs. III.C and V.

The form of the diffusion equation is unchanged from (2.1) or (2.6); and we shall simply use the symbols D and D' to denote the diffusion constants in the liquid and solid, respectively. The continuity condition is

$$v_n = D[\beta(\nabla u)_{\text{Solid}} - (\nabla u)_{\text{Liquid}}]\cdot\hat{n}, \tag{3.2}$$

where

$$\beta \equiv \begin{cases} D'c_p'/Dc_p & \text{(Thermal model)} \\ M'/M & \text{(Chemical model)}. \end{cases} \tag{3.3}$$

Finally, the Gibbs–Thomson condition can be written

$$u(\text{Interface}) = -d_0\mathcal{K}, \tag{3.4}$$

where d_0 is a capillary length defined by[4]

$$d_0 \equiv \begin{cases} \gamma T_M c_p/L^2 & \text{(Thermal model)} \\ \gamma/(\Delta C)^2(\partial\mu/\partial C) & \text{(Chemical model)}. \end{cases} \tag{3.5}$$

It will be convenient in some of the following discussion to talk in the language of the thermal model, that is, to call u the "temperature"; but it should be clear that the analysis applies equally well to the chemical case.

In the frame of reference moving in the z direction at the interface velocity v, the steady-state diffusion equation has the form:

$$\nabla^2 u + \frac{2}{l}\frac{\partial u}{\partial z} = 0, \tag{3.6}$$

where l is the diffusion length:

$$l = \frac{2D}{v}; \quad \left(l' = \frac{2D'}{v}\right). \tag{3.7}$$

The solution of (3.6) and the continuity condition (3.2) is:

$$u = \begin{cases} \exp\left(-\frac{2z}{l}\right) - 1 & \text{(Liquid, } z \geq 0) \\ 0 & \text{(Solid, } z \leq 0). \end{cases} \tag{3.8}$$

The flat interface has been placed at $z = 0$. Note that this steady-state solution exists for any positive v but requires a unit undercooling at infinity; that is, $u \to -1$ as $z \to +\infty$. The uniqueness of the undercooling is a result of the same conservation condition which allowed us to determine T_0 as a function of C_0 in Fig. 6; the interface must be warmed uniformly to the melting temperature by the released latent heat. For different undercoolings, no planar steady-state solutions exist. Note especially that the steady-state velocity v is not fixed by the undercooling. This is a situation which will recur in an important way in what follows.

The linear-stability analysis for this system can be performed in complete generality; but it will be best for purposes of this review to go directly to what is called the "quasistationary" approximation. We are looking for a linear equation of motion for the interfacial position, z (interface) $= \zeta(\mathbf{x},t)$, as defined in Eq. (2.13). In general, this equation contains memory effects; that is, a deformation of the interface causes a perturbation of the diffusion field which, in turn, affects the motion of the interface at later times. However, in most of the situations of interest here, it turns out that the interface moves so slowly that it remains effectively stationary during the time needed for relaxation of the diffusion field. Thus it seems reasonable to solve the problem approximately by, first, solving the time-independent diffusion equation (3.6) subject to the thermodynamic boundary condition (3.4) on the quasistationary interface $\zeta(\mathbf{x},t)$, and then inserting this result into the continuity condition (3.2) to find an explicit expression for $\partial\zeta/\partial t$. We shall use the method throughout this paper and shall test it for consistency in connection with the present stability analysis. A completely time-dependent treatment of certain planar instabilities may be found in Sekerka (1967a,b), Langer and Turski (1977), or Langer (1977).

Returning to the problem at hand, we carry out the quasistationary analysis as follows. Consider a small perturbation of the steady-state interface:

$$\zeta(\mathbf{x},t) = \hat{\zeta}_{\mathbf{k}} \exp(i\mathbf{k}\cdot\mathbf{x} + \omega_k t), \tag{3.9}$$

where $\mathbf{k}$ is a two-dimensional wave vector perpendicular to $\mathbf{v}$ and $\omega_{\mathbf{k}}$ is the amplification rate whose sign determines stability. The corresponding solution of the diffusion equation (3.6) and its (primed) analog for the solid must have the form:

$$\left.\begin{aligned} u(\text{Liquid}) &\cong \exp(-2z/l) - 1 + \hat{u}_{\mathbf{k}} \exp(i\mathbf{k}\cdot\mathbf{x} - qz + \omega_k t) \\ u'(\text{Solid}) &\cong \hat{u}'_{\mathbf{k}} \exp(i\mathbf{k}\cdot\mathbf{x} + q'z + \omega_k t) \end{aligned}\right\}, \tag{3.10}$$

where q and q' are the positive solutions of

$$\left.\begin{aligned} -(2/l)q + q^2 - k^2 &= 0 \\ (2/l)q' + q'^2 - k^2 &= 0 \end{aligned}\right\}. \tag{3.11}$$

The amplitudes $\hat{u}_{\mathbf{k}}$ and $\hat{u}'_{\mathbf{k}}$ are small, of order $\hat{\zeta}_{\mathbf{k}}$, and can be obtained by evaluating (3.10) at $z = \zeta$, linearizing, and imposing (3.4). The result is:

$$-(2/l)\hat{\zeta}_{\mathbf{k}} + \hat{u}_{\mathbf{k}} = \hat{u}'_{\mathbf{k}} = -d_0 k^2 \hat{\zeta}_{\mathbf{k}}. \tag{3.12}$$

With the same linearization, (3.2) becomes:

$$\omega_k \hat{\zeta}_{\mathbf{k}} = -(2v/l)\hat{\zeta}_{\mathbf{k}} + Dq\hat{u}_{\mathbf{k}} + \beta Dq'\hat{u}'_{\mathbf{k}}. \tag{3.13}$$

Finally,

$$\begin{aligned} \omega_k &= v[q - (2/l)] - D(q + \beta q')d_0 k^2 \\ &\cong kv\left[1 - \frac{1}{2}(1+\beta)d_0 l k^2\right], \end{aligned} \tag{3.14}$$

---

[4] There has been some confusion in the literature regarding evaluation of the capillary length, especially in the chemical model. The problem is that $\partial\mu/\partial C$ is not easily measured directly. A commonly encountered form (see Mullins and Sekerka, 1964) can be derived by using the Clausius–Clapeyron equation for the latent heat L of a solution:

$$L = -T_M(\Delta C)\left(\frac{d\mu}{dT}\right)_{\text{coex}}.$$

The quantity $(d\mu/dT)_{\text{coex}}$ is the slope of the coexistence line in the μ–T plane, which can also be written in the form

$$\left(\frac{d\mu}{dT}\right)_{\text{coex}} = \left(\frac{\partial\mu}{\partial C}\right)\frac{dC_{\text{eq}}}{dT} + \frac{\partial\mu}{\partial T}.$$

Solving for $(\partial\mu/\partial C)$ and substituting into (3.5), one obtains

$$d_0(\text{Chemical}) = \frac{\gamma\left|\frac{dC_{\text{eq}}}{dT}\right|}{(\Delta C)^2\left(\frac{L}{T_M\Delta C} + \frac{\partial\mu}{\partial T}\right)}.$$

For dilute solution, when ΔC is very small, the quantity $\partial\mu/\partial T$ may be neglected, so that

$$d_0(\text{Chemical}) \cong \frac{\gamma T_M}{(\Delta C)L}\left|\frac{dC_{\text{eq}}}{dT}\right| = \frac{1}{(\Delta C)}\left|\frac{dC_{\text{eq}}}{dT}\right|\frac{L}{c_p}\, d_0(\text{Thermal}).$$

Note that the chemical capillary length can be several orders of magnitude larger than the thermal capillary length.

where the second, approximate, form of ω_k is valid in the limit that $kl \gg 1$ so that $q \cong q' \cong k$.

Because the formula (3.14) contains most of the physics to be encountered in this essay, it is worth some extra attention. The formula consists of two parts: a positive, destabilizing term which is proportional to the velocity, and a negative, stabilizing term which contains the surface tension. To see how these terms arise, consider the planar and deformed interfaces illustrated in Fig. 8, parts (a) and (b), respectively. The thermal fields u are indicated by dashed isotherms on the left and are shown explicitly for points along the z axis on the right. The steady-state function given in Eq. (3.8) appears in the right-hand side of part (a). In the absence of capillarity, a forward bulge in the interface like that at point A in (b) steepens the thermal gradient in the fluid ahead of it, which means that heat flows rapidly away from the surface and the bulge grows unstably. Similarly, a depression like that at B tends to melt back. With finite surface tension, however, the curvatures in (3.4) are such that the temperature is reduced at A and increased at B; and the resulting heat flow from B to A tends to restore the flatness of the interface. It is the competition between these two effects that determines the sign of ω_k in (3.14), and thus the overall stability of the interface.

For the case considered here, the interface is always unstable at sufficiently long wavelengths. The wavenumber k_s at which ω_k vanishes, that is, the neutral stability point, sets a length scale for the problem. Using the second form of (3.14), we have:

$$\lambda_s \equiv 2\pi/k_s \cong 2\pi\alpha\sqrt{ld_0}\,, \tag{3.15}$$

where α is a dimensionless factor which is ordinarily of order unity:

$$\alpha = [(1+\beta)/2]^{1/2}\,. \tag{3.16}$$

The most rapidly growing deformation occurs at the wave number $k_s/\sqrt{3}$. It seems reasonable to guess that patterns which emerge from this instability will, at least initially, have a characteristic size of order λ_s. The capillary length d_0 is a microscopic length of order angstroms. (In Ising-like mean-field theories, d_0 is essentially the same as the correlation length or the interfacial thickness.) The diffusion length l is usually macroscopic, in which case λ_s is of order microns, and $l/\lambda_s = 2\pi k_s l \gg 1$. Because we are interested primarily in deformations on the scale of λ_s, this is just the condition that we need in order to justify using the approximate version of Eq. (3.14). The quasistationary assumption is also easy to justify for these wavelengths. The dominant instabilities have growth rates of order $\omega_{\max} \sim k_s v$; whereas the relaxation rates for corresponding perturbations of the diffusion field are $\omega_{\text{diff}} \sim D k_s^2$. Thus the ratio $\omega_{\text{diff}}/\omega_{\max}$ is of order $k_s l \gg 1$, as required. Conversely, when one encounters situations in which $k_s l$ is small, that is, when the wavelength of the deformation is comparable to or larger than l, then the quasistationary approximation is invalid except for strictly stationary states of the system.

B. Pure substance: growing sphere

The second simple case that will be useful to consider is that of a solid sphere of a pure substance immersed in an undercooled melt (see Mullins and

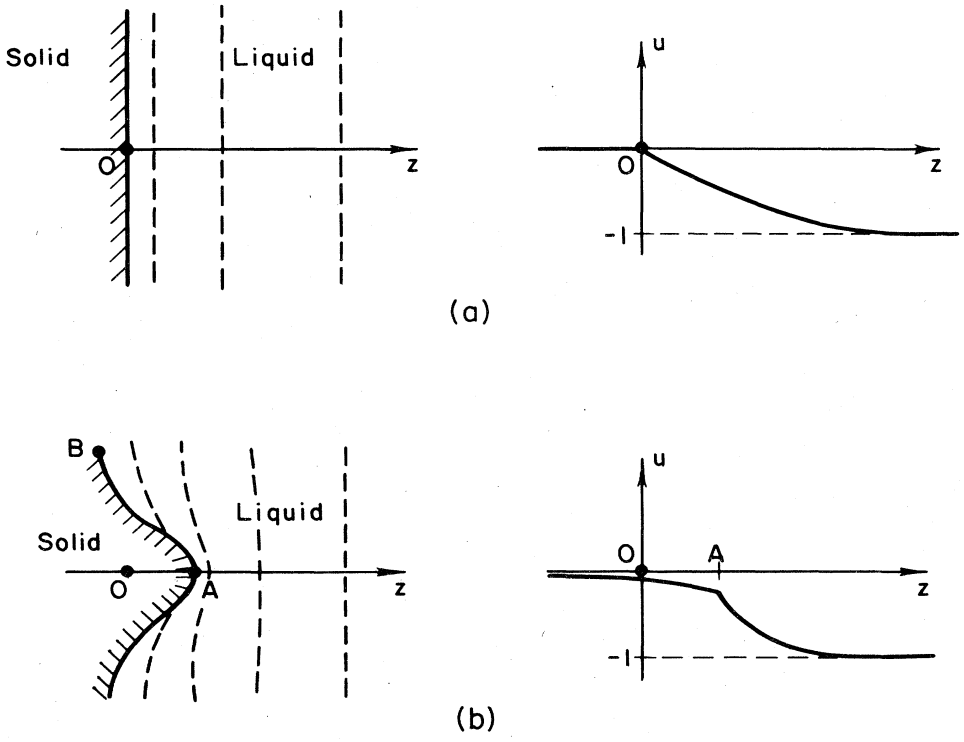

FIG. 8. Schematic illustration of the Mullins–Sekerka instability.

Sekerka, 1963). There is no true steady-state solution in this geometry, because the rate of growth of the sphere depends upon its radius which is increasing with time. What is interesting to study is the spherical shape-preserving mode of growth, which is the quiescent state for our purposes, and the manner in which this mode becomes unstable.

Consider first the purely spherical situation. Let the radius of the sphere be R_0, and let the undercooling at infinity be Δ; that is

$$u(\infty) = -\Delta . \tag{3.17}$$

In the quasistationary approximation, the diffusion field simply satisfies Laplace's equation everywhere; thus

$$u_0(r) = \begin{cases} -\Delta + \dfrac{R_0}{r}\left(\Delta - \dfrac{2d_0}{r}\right), & r > R_0; \\ -\dfrac{2d_0}{R_0}, & r \leq R_0; \end{cases} \tag{3.18}$$

where r is the radius measured from the center of the sphere, and the boundary condition (3.4) has been imposed at $r = R_0$. The continuity condition (3.2) determines the growth rate:

$$v_R \equiv \frac{dR_0}{dt} = \frac{D}{R_0}\left(\Delta - \frac{2d_0}{R_0}\right). \tag{3.19}$$

Next, consider a slightly deformed sphere whose radius R is given, in terms of the polar coordinates θ and ϕ, by

$$R(\theta, \phi) = R_0 + \delta_j Y_{j,m}(\theta, \phi)\exp(\omega_j t), \tag{3.20}$$

where δ_j is the small deformation amplitude, and $Y_{j,m}$ is the spherical harmonic of order j, m. Associated with this deformation is a diffusion field of the form

$$u(r, \theta, \phi) = u_0(r) + u_j(r) Y_{j,m}(\theta, \phi)\exp(\omega_j t), \tag{3.21}$$

where

$$u_j(r) = \begin{cases} (a_j / r^{j+1}) (\text{Liquid}, & r > R) \\ b_j r^j (\text{solid}, & r \leq R). \end{cases} \tag{3.22}$$

We calculate the coefficients a_j and b_j by evaluating (3.21) at $r = R$, linearizing and imposing the boundary condition (3.4). To do this, we must know that the curvature in spherical coordinates is

$$\mathcal{K} \cong \frac{2}{R} + \frac{1}{R^2}\Lambda R + \dots , \tag{3.23}$$

where Λ is the angular part of the Laplacian whose eigenstates are $Y_{j,m}$ with eigenvalues $j(j+1)$. The result is

$$-\frac{v_R}{D}\delta_j + \frac{a_j}{R_0^{j+1}} = b_j R_0^j = -\frac{d_0}{R_0^2}(j-1)(j+2)\delta_j . \tag{3.24}$$

In a similar way, the continuity condition (3.2) becomes:

$$\omega_j \delta_j = -\frac{2v_R}{R_0}\delta_j + \frac{(j+1)Da_j}{R_0^{j+2}} + j\beta D R_0^{j-1} b_j . \tag{3.25}$$

Equations (3.24) and (3.25) have been written here as direct analogs of (3.12) and (3.13). From these, we obtain the amplification rate:

$$\omega_j = \frac{(j-1)v_R}{R_0}\left\{1 - \left(1 + \frac{1}{j} + \beta\right)\frac{Dd_0 j(j+2)}{v_R R_0^2}\right\}, \tag{3.26}$$

which bears a close resemblance to (3.14) and, indeed, is identical to the latter equation in the limit of finite wavelengths on a large sphere, that is, in the limit $R_0 \to \infty, j \to \infty, j/R_0 = k$.

Equation (3.26) has been expressed in terms of the local growth velocity v_R instead of Δ, the undercooling at infinity. This form of the relation points up the similarity to the planar case and will be particularly useful later in our discussion of the dendritic instabilities; but it obscures the most direct interpretation of this analysis. To see what is happening to the sphere as it grows, let us use Eq. (3.19) to eliminate v_R in favor of the critical radius R^*

$$R^* \equiv 2d_0/\Delta . \tag{3.27}$$

Readers will recognize R^* as the critical radius for nucleation, that is, the minimum radius at which a droplet will grow rather than melt at the given undercooling. If R_0 is just slightly larger than R^*, then v_R is small and positive, and ω_j as given in (3.26) must be negative for any j—the sphere is completely stable. The interesting quantity to compute is the radius at which the sphere becomes unstable. Let us define R_j^* to be the neutral stability radius for the jth mode, that is, the value of R_0 at which ω_j vanishes. We find:

$$\frac{R_j^*}{R^*} = 1 + \frac{1}{2}\left(1 + \frac{1}{j} + \beta\right) j(j+2); \quad j \geq 2 . \tag{3.28}$$

The smallest R_j^* occurs for $j = 2$; thus, for the metallurgically interesting chemical case where $\beta \ll 1$, this first instability sets in at $R_0 = 7R^*$. Spheres of this size are really quite small. The capillary length d_0 is usually of order angstroms, and characteristic values of Δ are of order 10^{-2}. It is not certain how large the sphere must be before the size of the deformation becomes comparable to the sphere itself—we shall need a full nonlinear theory plus some analysis of the thermal fluctuations which drive the instability before we can answer such questions. But it seems likely that dendrite-forming instabilities originate with crystalline seeds typically in the submicron range.

C. Directional solidification

We return now to the planar situation and reintroduce the controlling thermal gradient described in Sec. II.C. The necessary linear-stability analysis is much the same as in III.A. The appropriate dimensionless diffusion field, u, is defined in Eq. (3.1) (chemical model) with $\tilde{\mu}$ defined in (2.11). For purposes of our linear analysis, we replace (ΔC) in (3.1) by (ΔC_0), the width of the miscibility gap at the reference temperature T_0. Because the gap is no longer constant, however, we must rewrite the continuity equation (3.2) in the form:

$$\left(\frac{\Delta C}{\Delta C_0}\right) v_n = D[\beta(\nabla u)_{\text{Solid}} - (\nabla u)_{\text{Liquid}}] \cdot \hat{n}, \tag{3.29}$$

where

$$\left(\frac{\Delta C}{\Delta C_0}\right)\cong 1-\frac{(1-K)}{l_T}\zeta+\left(\frac{\mu_c}{\mu_c'}-1\right)d_0\mathcal{K}\ . \tag{3.30}$$

Here we have introduced the quantities:

$$K\equiv\left|\frac{dC_{eq}'}{dT}\right|\Big/\left|\frac{dC_{eq}}{dT}\right|\ , \tag{3.31}$$

which becomes the conventional partition coefficient for dilute solutions, and

$$\frac{\mu_C}{\mu_C'}\equiv\left(\frac{\partial\mu}{\partial C}\right)\Big|_{C=C_{eq}}\Big/\left(\frac{\partial\mu}{\partial C}\right)'\Big|_{C=C_{eq}'}\ . \tag{3.32}$$

The thermal length l_T is defined by

$$\frac{1}{l_T}\equiv\frac{G}{(\Delta C_0)}\left|\frac{dC_{eq}}{dT}\right|\ . \tag{3.33}$$

We shall also need the analogous quantity

$$\frac{1}{l_T'}\equiv\frac{D'G}{\beta D(\Delta C_0)}\left|\frac{dC_{eq}'}{dT}\right|\ . \tag{3.34}$$

The second and third terms on the right-hand side of (3.30) describe changes in ΔC due, respectively, to displacement of the interface relative to the thermal gradient and to the Gibbs–Thomson effect.

The solutions of the diffusion equation are again given by (3.10) and (3.11); and the thermodynamic boundary conditions analogous to (3.12) are obtained from (2.16):

$$\left.\begin{aligned} u(\text{Liquid interface}) &= -d_0\mathcal{K}-\frac{1}{l_T}\zeta \\ u(\text{Solid interface}) &= -d_0\mathcal{K}-\frac{1}{l_T'}\zeta \end{aligned}\right\}. \tag{3.35}$$

After some algebra, one finds

$$\begin{aligned}\omega_k &= v\left(q-\frac{2}{l}\right)-\frac{Dq}{l_T}-\frac{\beta Dq'}{l_T'}+\frac{2(1-K)D}{ll_T} \\ &\quad-\left[q+\beta q'-\frac{2}{l}\left(1-\frac{\mu_c}{\mu_c'}\right)\right]Dd_0k^2 \\ &\cong kv\left[1-\frac{l}{2}\left(\frac{1}{l_T}+\frac{\beta}{l_T'}\right)-\frac{1}{2}(1+\beta)d_0lk^2\right],\end{aligned} \tag{3.36}$$

where q and q' are defined in (3.11). As before, the approximate version of (3.36) is valid when $kl\gg 1$.

The obvious new feature of this formula is the k-independent, stabilizing (i.e., negative) term inside the brackets, which we shall denote by ν^{-1}:

$$\frac{1}{\nu}\equiv\frac{l}{2}\left(\frac{1}{l_T}+\frac{\beta}{l_T'}\right)=\frac{G}{v(\Delta C_0)}\left(D\left|\frac{dC_{eq}}{dT}\right|+D'\left|\frac{dC_{eq}'}{dT}\right|\right). \tag{3.37}$$

According to the second version of (3.36), the interface is completely stable as long as

$$\nu<\nu_C\cong 1.\quad\text{(Stability)} \tag{3.38}$$

In this approximation, the first instabilities seem to occur near $k=0$ when ν exceeds unity; but the approximation is not accurate at such long wavelengths. Closer examination of the exact formula (3.36) reveals that the onset of instability occurs at a finite k, and that the critical ν exceeds unity by an amount which depends on the surface tension but which ordinarily is small (see Sec. V.) Let us assume that (3.38) is accurate. Then, in the metallurgically interesting case where $D'\ll D$, this stability criterion looks precisely the same as constitutional supercooling. To see this, note that the steady-state concentration gradient just ahead of the planar interface is $v(\Delta C_0)/D$; thus the condition that the dashed C vs T curve in Fig. 6 remains outside of the two-phase region is

$$\frac{v(\Delta C_0)}{DG}<\left|\frac{dC_{eq}}{dT}\right|.\quad\text{(Stability, }D'=0\text{)}. \tag{3.39}$$

For metallurgical purposes, this is a good rule of thumb for estimating stability limits, at least for this particular class of problems. From a theoretical point of view, however, the criterion can be misleading because the instability actually involves a more complex interplay of kinetic effects than is contained in the simple thermodynamic interpretation of (3.39). Even without capillary corrections, Eqs. (3.37) and (3.38) imply that an appreciable diffusivity in the solid can stabilize the interface against a certain degree of supercooling in the adjacent fluid.

The quantity ν is a dimensionless group of parameters which plays the same role here as do the Rayleigh or Reynolds numbers in hydrodynamics. The system is quiescent at small ν and passes through cellular and dendritic stages as ν becomes larger. To increase ν experimentally, one either increases the velocity v, decreases the thermal gradient G, or changes the solute concentration in such a way as to increase the miscibility gap (ΔC_0). The theoretical problem of predicting the shapes of nonplanar solidification fronts at supercritical values of ν will be discussed in Sec. V.

IV. DENDRITIC GROWTH

A. The needle crystal

In dealing with the dendrite problem, we are going to proceed exactly as we did in the planar or spherical cases; that is, we are going to find a quiescent state of the system and then examine the linear equations of motion for perturbations of this state. The mathematics will be more complicated than before; and we shall emerge with a picture of a phenomenon which is intrinsically time dependent and nonlinear. But the actual analysis will be no different in principle from that of the last section.

The artificial snowflake shown in Fig. 3 presumably started forming when its central seed became unstable in the manner described in Sec. III.B; and its subsequent growth was governed by the full nonlinear equations appropriate for the simple thermal model. From direct observation, we know that the tips of each of the six primary dendrites move outward at constant speed—a speed that we should like to be able to predict. Moreover, the measured values of v indicate that the characteristic range of the diffusion field, $l=2D/v$, while generally very much larger than the scale of the microstructure near the tip, is appreciably smaller than the spacing between primary tips. Thus each primary dendrite may be considered to be growing, by itself, into its own uniformly undercooled environment. In a frame of reference which is moving at constant velocity with the tip, the dendritic structure still appears to be

time dependent because of the sidebranching activity. But, if one either neglects the sidebranches altogether or assumes that it is only some sort of time-averaged shape which matters, one arrives at a model in which a relatively simple, "needle"-shaped solidification front remains stationary in the moving frame.

A schematic drawing of the tip of a needle crystal is shown in Fig. 9. Remember that the planar interface is inconsistent with steady-state heat conservation for any undercooling Δ other than unity [see Eq. (3.17)]. At the small undercoolings of interest here, the solidification front must bend back so that the thermal flux (normal to the dashed isotherms shown in the figure) diverges from the leading edge of the tip where the latent heat is being generated. Unfortunately, analytic steady-state solutions of this problem are known only in the case of zero surface tension, where the interface is always at the bulk melting temperature. The known solutions are paraboloids of either circular (Ivantsov, 1947) or elliptical (Horvay and Cahn, 1961) cross sections. These isothermal solutions are going to play an important role in what follows.

Let us restrict ourselves to three-dimensional situations in which the steady-state solutions have cylindrical symmetry about the growth axis of the dendrite. (The stability analysis has not yet been performed for the more general elliptic case.) We define a system of parabolic coordinates ξ, η, θ, moving with the tip of the dendrite, as shown in Fig. 10:

$$\xi = (r - z)/\rho; \quad \eta = (r + z)/\rho . \tag{4.1}$$

Here, r is the radial distance measured from the origin O; and ρ is the radius of curvature at the tip of the parabola defined by $\eta = 1$. The angle θ measures rotations about the z axis. In terms of these variables, the quasistationary diffusion equation becomes:

$$\frac{1}{\eta+\xi}\left(\frac{\partial}{\partial\eta}\eta\frac{\partial u}{\partial\eta}+\frac{\partial}{\partial\xi}\xi\frac{\partial u}{\partial\xi}\right)+\frac{1}{4\eta\xi}\frac{\partial^2 u}{\partial\theta^2}+\frac{p}{\eta+\xi}\left(\eta\frac{\partial u}{\partial\eta}-\xi\frac{\partial u}{\partial\xi}\right)=0, \tag{4.2}$$

where u is the dimensionless diffusion field defined previously; and

$$p \equiv \rho v/2D = \rho/l \quad (p' \equiv \rho v/2D') \tag{4.3}$$

is known as a Péclet number. The instantaneous position of the interface will be given by $\eta_s(\xi, \theta, \tau)$, where

$$\tau \equiv 2vt/\rho . \tag{4.4}$$

Then the continuity condition (3.2) becomes

$$\eta_s + \xi\frac{\partial\eta_s}{\partial\xi} + (\eta_s+\xi)\frac{\partial\eta_s}{\partial\tau} = \frac{\beta}{p}\,\Xi\,[\eta\to\eta_s(\text{Solid})] - \frac{1}{p}\,\Xi\,[\eta\to\eta_s(\text{Liquid})], \tag{4.5}$$

where

$$\Xi = \eta_s\frac{\partial u}{\partial\eta} - \xi\frac{\partial\eta_s}{\partial\xi}\frac{\partial u}{\partial\xi} - \frac{\eta_s+\xi}{4\eta_s\xi}\frac{\partial\eta_s}{\partial\theta}\frac{\partial u}{\partial\theta} . \tag{4.6}$$

In the absence of capillarity, the thermodynamic boundary condition requires simply that u vanish on the interface. In this case, there exists a stationary solution of (4.2) and (4.5) with $\eta_s = 1$, for which the diffusion field $u = u_s$ is a function only of η:

$$u_s = \begin{cases} 0, & \eta \le 1 \\ -\Delta + \dfrac{\Delta}{E_1(p)}E_1(p\eta), & \eta > 1, \end{cases} \tag{4.7}$$

where E_1 is the exponential integral:

$$E_1(y) = \int_y^\infty \frac{e^{-y'}}{y'}dy' . \tag{4.8}$$

This field is consistent with (4.5) as long as

$$\Delta = pe^p E_1(p) . \tag{4.9}$$

Equation (4.9) represents the full content of the zero-capillarity, steady-state hypothesis—the undercooling Δ determines p and thus fixes only the product of the parameters v and ρ. Of course, a complete theory must

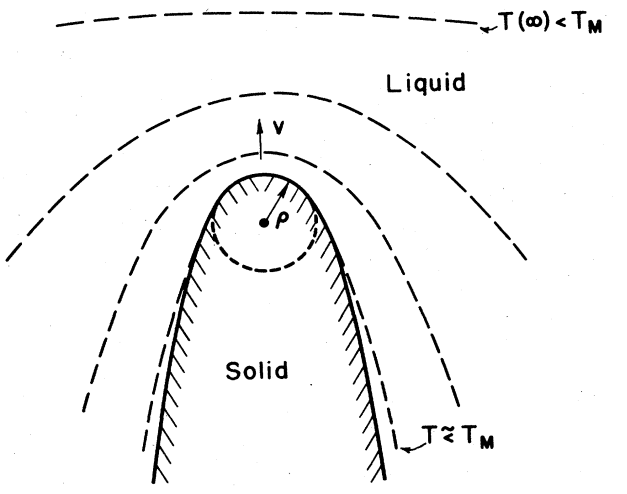

FIG. 9. Schematic picture of a needle crystal with a spherical tip.

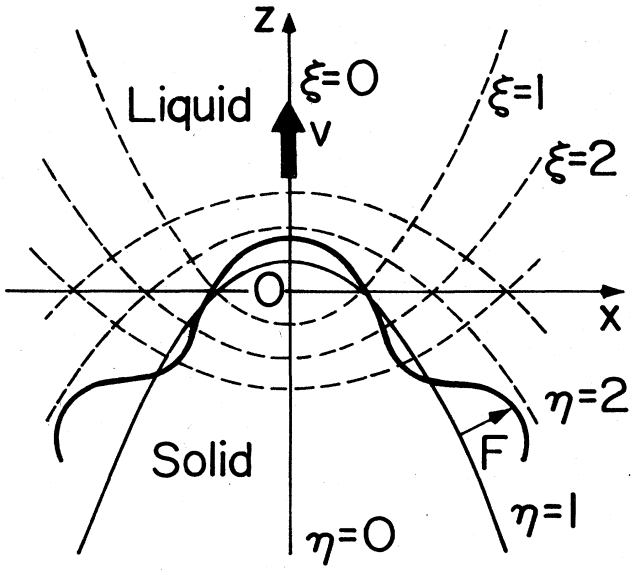

FIG. 10. Parabolic coordinate system used for stability analyses.

predict separately both of these parameters.

Much of the recent history of the dendrite problem consists of attempts to introduce capillarity into the steady-state needle-crystal model, the hope being that one might discover some property of the solution which will identify a natural growth rate. The easiest way to understand the effect of capillarity is to go back to a simple approximation originally suggested by Fisher (see Chalmers, 1964). Just in front of the tip of the dendrite, the temperature field shown in Fig. 9 looks roughly like that in the neighborhood of a growing sphere of the kind discussed in Sec. III.B. This picture suggests that we use Eq. (3.19) to write

$$v \cong \frac{D}{\rho}\left(\Delta - \frac{2d_0}{\rho}\right), \tag{4.10}$$

where we have simply identified the forward velocity at the front of the dendrite with the radial growth rate of the sphere. Equation (4.10) is illustrated in Fig. 11 along with the Ivantsov result and two more accurate approximations which we shall describe shortly. The effect of surface tension is to reduce v appreciably for small values of ρ. Most notably, v passes through a maximum at $\rho = 2R^*$, where R^* is the critical nucleation radius defined in (3.27). It frequently has been conjectured in the metallurgical literature that the maximum velocity locates the natural operating point of the dendrite. This hypothesis now appears to be incorrect, but it has served as a theoretical framework for much of the research on solidification during the past twenty years and, in this role, has stimulated some very useful investigations.

Equation (4.10) is not a very good approximation to the true $v-\rho$ curve, but possesses most of the qualitative features of the exact steady-state theory. In addition to exhibiting a maximum in v, the equation illustrates the general scaling law:

$$v = (2D/d_0)V(\Delta, \tilde{\rho}), \quad \tilde{\rho} \equiv \rho/d_0; \tag{4.11}$$

or alternatively:

$$\Delta = \Delta(\tilde{\rho}, V), \tag{4.12}$$

where V and Δ are dimensionless functions of their arguments and may, in addition, depend on β. The difficulty in obtaining the exact relationship is that, because of the Gibbs–Thomson condition (3.4), the steady-state solidification fronts are neither isothermal nor exactly paraboloidal. Nash and Glicksman (1974) have developed a numerical technique for solving this problem, but so far have used their method only to compute maximum velocities rather than, say, complete $V-\tilde{\rho}$ curves for various values of Δ. Two approximate calculations are of special interest because they are based on the Ivantsov solution and are consistent with it in the limit of large $\tilde{\rho}$. Both of these approximations assume an exactly paraboloidal dendrite, and then adjust for this assumption by partially relaxing either the thermodynamic boundary condition (3.4) or the continuity condition (3.2). In the "modified Ivantsov" method of Sekerka *et al.* (1967), the ξ-dependent curvature in (3.4) is replaced by the constant value $2/\rho$. The interface is still isothermal, so the steady state is unaffected by heat flow in the solid. One finds simply

$$\Delta = 2/\tilde{\rho} + pe^{p}E_1(p); \quad (p = \tilde{\rho}V). \tag{4.13}$$

The Temkin method (Temkin, 1960) preserves (3.4)

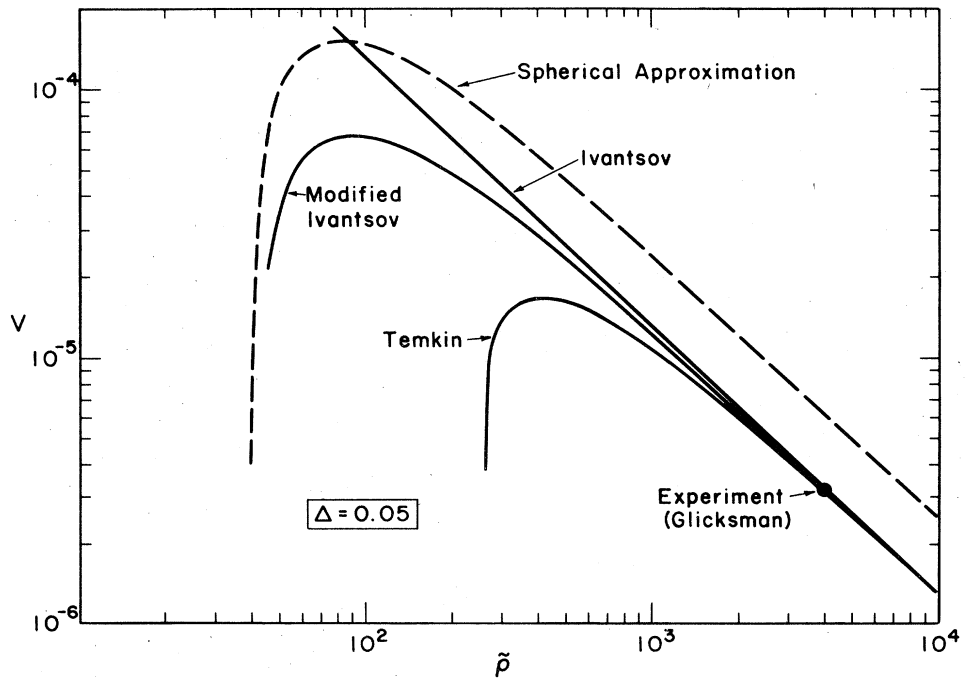

FIG. 11. Dimensionless dendritic growth velocity, $V = vd_0/2D$, as a function of tip radius, $\tilde{\rho} = \rho/d_0$, for a dimensionless undercooling $\Delta = (T_M - T)c_p/L = 0.05$, determined by the four steady-state approximations as indicated. The experimental point (solid circle) has been provided by Glicksman (to be published) from recent measurements on succinonitrile.

in the form

$$u(\text{Interface}) = -\frac{d_0}{\rho}\frac{2+\xi}{(1+\xi)^{3/2}}, \tag{4.14}$$

where the right-hand side is the correct curvature for a paraboloid of revolution, but imposes the continuity condition (3.2) only at $\xi = 0$. The result is:

$$\Delta = [1+(b/\tilde{\rho}^2 V)]\, pe^p E_1(p), \tag{4.15}$$

where

$$b \cong \begin{cases} 1.819; & D' = 0, \quad \beta = 0; \\ 2.949; & D' = D, \quad \beta = 1. \end{cases} \tag{4.16}$$

The quantity b is actually the small-p limit of a weakly p-dependent function (Trivedi, 1970). Equations (4.13) and (4.15) are illustrated in Fig. 11 for the case $\Delta = 0.05$.

By far the most important investigation which has been stimulated by the needle-crystal theory is the experimental work of Glicksman *et al.* (1976) on succinonitrile dendrites. The basic scheme of this experiment was described in Sec. II.A. Succinonitrile was chosen because of its convenient melting temperature, cubic symmetry, and relatively small latent heat which, it was hoped, would minimize anisotropies associated with attachment kinetics. To my knowledge, this is the only experiment in which ρ has been measured as well as v, so that the steady-state theory can be tested independently of the maximum-velocity hypothesis. To indicate the nature of the results, I have marked the experimental $\tilde{\rho} - V$ point for $\Delta = 0.05$ in Fig. 11. Figure 12 is a multiple-exposure photograph of a downward-growing dendrite tip from which one can measure ρ and v and also observe the sidebranching mechanism.

The results of these experiments are clear and very interesting. When observed closely, as in Fig. 12, the succinonitrile dendrites exhibit smooth, paraboloidal tips. There is always sidebranching activity, which emerges within a distance of a few radii ρ behind the tip and, initially, consists of a smooth surface undulation with a well-defined wavelength of order ρ. At larger distances from the tip, these deformations coarsen and grow out into well-developed sidebranches whose spacing is considerably larger than the initial wavelength. In the immediate vicinity of the tip, however, the core of the dendritic structure looks very much like a paraboloid of revolution. It seems to be generally true at all accessible undercoolings that the experimental point (ρ, v) lies on or near the steady-state curve—as in Fig. 11—at a place where $\tilde{\rho}$ is so large that the difference between the Ivantsov result (4.9) and the capillary modifications (4.13) and (4.15) is no more than a few percent. These experimental points deviate from the most reliable maximum-velocity predictions (Nash and Glicksman, 1974) by factors of 5 or more in both ρ and v. Thus there is a clear contradiction of the maximum-velocity hypothesis; but the underlying steady-state, needle-crystal model seems to be valid. Best of all from a theoretical point of view, the natural operating point of the dendrite seems to correspond to a nearly isothermal needle crystal—one whose shape

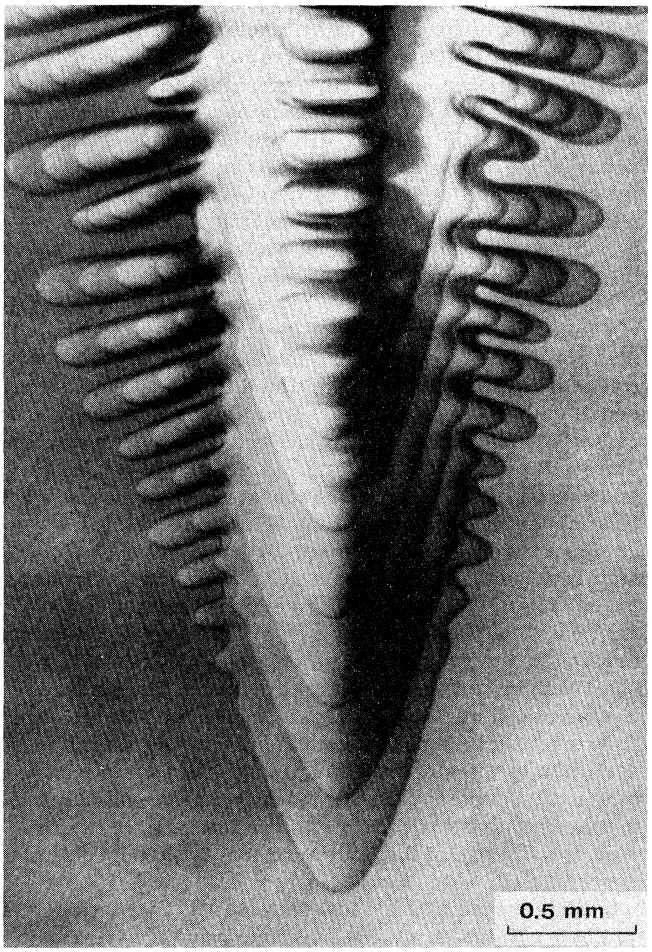

FIG. 12. Multiple-exposure photograph of a downward-growing succinonitrile dendrite (Glicksman, to be published).

is not much affected by capillarity. The obvious question is: how does nature choose this particular operating point? As one might guess, the answer to this question has to do with stability.

B. Dendritic instabilities

The idea that instabilities and associated nonstationary processes might play an essential role in dendritic crystal growth is by no means a new one. Glicksman *et al.* (1976), in their test of the maximum-velocity theory, postulated that time-dependent considerations may be necessary in order to understand their data. Holtzmann (1969) emphasized the potential importance of a stability analysis in the introduction to his thesis, and predicted that the ultimately correct mathematical model of dendritic growth will exhibit periodic motion of some sort. Oldfield (1973), in connection with his numerical studies of the dendrite, proposed a simple stability criterion which turns out to be similar in its basic idea to what will be described below.

In the following paragraphs, I shall summarize some results that have been obtained recently by Müller-Krumbhaar and myself (Langer and Müller-Krumbhaar,

1977, 1978). This work is by no means complete, but the basic features seem to fit together so neatly that I think they belong as a central feature of this essay. The mathematics has a 19th century flavor which I shall try to convey without including all the technical details. (Serious readers will find a more thorough description of the analysis in the original papers.) In order to make the procedure as clear as possible, I shall present each step as a direct analog of a corresponding step in the solution of the simple planar stability problem [Eqs. (3.8) through (3.14)].

The key to a feasible stability analysis for the dendrite is the expected small size of the capillarity induced, steady-state shape corrections. Strictly speaking, the linear perturbation theory outlined in Sec. III makes sense only if the shape correction is known exactly and can be incorporated into the description of the quiescent state whose stability is being examined. Because the correction is small, it can accurately be evaluated to first order in the surface tension and the result used to compute a corresponding first-order correction to the stability equation. Even this relatively straightforward procedure is computationally very difficult, and may turn out to be feasible only in a simple two-dimensional version of the problem. The only calculations that I shall report here are those in which the shape correction has been neglected altogether. These are the calculations which lead to a convincing mathematical description of the sidebranching instability; and their internal consistency lies in the fact that the sidebranching modes have very little of their intensity in the immediate vicinity of the tip where the shape correction is appreciable.

In the absence of a steady-state shape correction, the quiescent diffusion field—analogous to (3.8)—remains as given by Eq. (4.7). The perturbation of the interface, the analog of (3.9), can be described in the form

$$\eta_s(\xi,\theta,t)-1=F_m(\xi,\tau)\exp(im\theta);\quad m=\text{integer};\qquad (4.17)$$

where τ is the timelike variable defined in (4.4); and we have taken advantage of the cylindrical symmetry to presume a periodic θ dependence of the deformation. The function F is actually a parabolic coordinate, but may conveniently be visualized as the normal displacement indicated in Fig. 10. In contrast to (3.9), we have not immediately assumed an exponential τ dependence of F in (4.17) because, for reasons which will become clear, we shall want to supplement the previous kind of eigenvalue analysis with a direct study of the time dependence of certain perturbations.

This problem has no special symmetry in the z direction; therefore we cannot *a priori* assume any particular ξ dependence of F, nor can we avoid the construction of a general solution of the quasistationary diffusion equation (4.2). The best we can do in analogy to (3.10) is to take advantage of the separability of (4.2) and write

$$\left.\begin{aligned} u(\text{Liquid})&=u_s(\eta)+\sum_{n=0}^{\infty}a_nW_{n,m}(p\eta)(p\xi)^{|m|/2}L_n^{|m|}(p\xi)e^{im\theta}\\ u(\text{Solid})&=\sum_{n=0}^{\infty}b_nW'_{n,m}(p'\eta)(p'\xi)^{|m|/2}L_n^{|m|}(p'\xi)e^{im\theta}\end{aligned}\right\};\qquad (4.18)$$

where the L's are associated Laguerre polynomials, and the W's are confluent hypergeometric functions which satisfy

$$w\frac{d^2W_{n,m}}{dw^2}+(1+w)\frac{dW_{n,m}}{dw}-\left(n+\frac{|m|}{2}+\frac{m^2}{4w}\right)W_{n,m}=0.\qquad (4.19)$$

The separation constants (integer n) have been chosen so that the diffusion field is well behaved along $\xi=0$. Then the solutions to (4.19) are uniquely determined by the conditions that, in the liquid, W must vanish for $\eta\to\infty$ and, in the solid, W' must be regular at $\eta=0$.

The coefficients a_n and b_n are understood to be first order in the perturbation F. The next step, in analogy to (3.12), is to evaluate these coefficients by imposing the Gibbs–Thomson condition at the interface. To do this, we need to know the curvature $\mathcal{K}$ in parabolic coordinates to first order in F. The required formula is:

$$\mathcal{K}\cong\frac{1}{\rho}[K^{(0)}-K^{(1)}F_me^{im\theta}+\ldots]\qquad (4.20)$$

where $K^{(0)}$ is the coefficient of d_0/ρ on the right-hand side of (4.14), and

$$K^{(1)}F_m=\frac{2\xi}{(1+\xi)^{1/2}}\frac{d^2F_m}{d\xi^2}+\frac{2+3\xi}{(1+\xi)^{3/2}}\frac{dF_m}{d\xi}+\frac{4+2\xi+\xi^2}{2(1+\xi)^{5/2}}F_m-\frac{m^2}{2\xi}(1+\xi)^{1/2}F_m.\qquad (4.21)$$

Then the analog of (3.12) is

$$-pF_m(\xi)+\sum_{n=0}^{\infty}a_nW_{n,m}(p)(p\xi)^{|m|/2}L_n^{|m|}(p\xi)=\sum_{n=0}^{\infty}b_nW'_{n,m}(p')(p'\xi)^{|m|/2}L_n^{|m|}(p'\xi)=\frac{d_0}{\rho}K^{(1)}F_m(\xi).\qquad (4.22)$$

Similarly, the analog of the continuity equation (3.13) is found by inserting (4.18) into (4.5) and linearizing:

$$(1+\xi)\frac{\partial F_m}{\partial\tau}=-(1+p)F_m-\xi\frac{\partial F_m}{\partial\xi}+\frac{\beta D}{D'}\times\sum_{n=0}^{\infty}b_n\frac{\partial W'_{n,m}(p')}{\partial p'}(p'\xi)^{|m|/2}L_n^{|m|}(p'\xi)-\sum_{n=0}^{\infty}a_n\frac{\partial W_{n,m}(p)}{\partial p}(p\xi)^{|m|/2}L_n^{|m|}(p\xi).\qquad (4.23)$$

The coefficients a_n and b_n are obtained in terms of $F_m(\xi)$ by using the orthogonality of the Laguerre functions in (4.22). The equation of motion for F_m, which results from substituting the expressions for a_n and b_n into (4.23), contains divergent and generally unpleasant sums over special functions. To make further progress, Müller–Krumbhaar and I have taken the limit $p\to 0$. This is an experimentally justified approximation; observed values of p are in the range 0.01–0.1 for the succinonitrile experiments and are an order of magnitude smaller than that for Fujioka's ice dendrites. In this limit, the sums over n in (4.23) become integrals and, after a bit of manipulation, we obtain:

$$(1+\xi)\frac{\partial F_m}{\partial \tau} = -\frac{\partial}{\partial \xi}(\xi F_m) + \int_0^\infty G_m(\xi,\xi')[1+\sigma K^{(1)}]F_m(\xi')d\xi' + \int_0^\infty G'_m(\xi,\xi')\sigma' K^{(1)}F_m(\xi')d\xi' ; \quad (4.24)$$

where

$$G_m(\xi,\xi') = \int_0^\infty d\mu\left[-\mu\frac{d}{d\mu}\ln K_m(2\sqrt{\mu})\right]J_m(2\sqrt{\mu\xi})J_m(2\sqrt{\mu\xi'}) ; \quad (4.25)$$

and

$$G'_m(\xi,\xi') = \int_0^\infty d\mu\left[\mu\frac{d}{d\mu}\ln I_m(2\sqrt{\mu})\right]J_m(2\sqrt{\mu\xi})J_m(2\sqrt{\mu\xi'}) . \quad (4.26)$$

The J_m, K_m, and I_m are the conventional ordinary and modified Bessel functions (Abramowitz and Stegun, 1964).

Once the limit $p \to 0$ has been taken in (4.24), the only system parameters remaining in the stability problem are:

$$\left.\begin{aligned}\sigma &= \frac{2d_0D}{\rho^2 v} \equiv \left(\frac{\lambda_s}{2\pi\rho}\right)^2 ;\\ \sigma' &= \beta\sigma ;\end{aligned}\right\} \quad (4.27)$$

where λ_s is a stability length defined in analogy to (3.15):

$$\lambda_s \equiv 2\pi\sqrt{d_0 l} . \quad (4.28)$$

We have arrived here at a very general feature of the dendrite problem—a feature which persists when the shape correction is taken into account and which is, in fact, a simple consequence of dimensional considerations. The removal of the Pêclet number p from the stability analysis means that the diffusion length has been taken to be so large that it scales out of the problem. This leaves us with only two lengths in the system: the tip radius ρ and the stability length λ_s; and only the ratio of these lengths can enter into a properly scaled theory. Therefore, if the operating point of the dendrite is to be determined by a stability criterion, then that criterion must have the form [see (4.11)]:

$$\sigma = \frac{2d_0D}{\rho^2 v} = \frac{1}{\tilde{\rho}^2 V} = \sigma^* , \quad (4.29)$$

where σ^* is a constant which may depend on β, but not on dynamic quantities like ρ or v. In conjunction with a $\tilde{\rho} - V$ relation of the form (4.11) or (4.12), Eq. (4.29) would constitute a solution of the dendrite problem in that it would allow us to predict both $\tilde{\rho}$ and V as functions of Δ. It remains to show that a stability mechanism really exists, and then to compute a value for σ^*. To do this, we must return to the equation of motion (4.24).

It is useful to think of the parameter σ as locating a point along the steady-state $\tilde{\rho} - V$ curve. Small values of σ correspond to slow, fat dendrites for which capillarity is unimportant; and larger values specify sharper dendrites with greater growth velocities. The stability problem (4.24) is soluble analytically in the Ivantsov limit, $\sigma = 0$. Unfortunately, the curvature operator in (4.24) constitutes a singular perturbation, and we cannot use this exact solution as a starting point for an approximation scheme; but the result is of interest by itself.

With $\sigma = 0$, Eq. (4.24) can be solved in the sense that one can find characteristic modes of the form

$$F_m(\xi,\tau) = e^{\Omega\tau}F_{m,\Omega}(\xi) \quad (4.30)$$

for all real, positive values of Ω. The equation is solved by performing a Fourier–Bessel transformation:

$$F_{m,\Omega}(\xi) = \int_0^\infty d\mu\phi_{m,\Omega}(\mu)J_m(2\sqrt{\mu\xi}) , \quad (4.31)$$

which, for $\sigma = 0$, reduces (4.24) to a differential equation for $\phi(\mu)$. The solution of that equation can be written in the form:

$$\phi_{m,\Omega}(\mu) = K_m(2\sqrt{\mu})\int_0^\mu d\mu' \frac{e^{-\mu'/\Omega}}{\mu' K_m^2(2\sqrt{\mu'})} . \quad (4.32)$$

To make sense of this result, it is best to look in the limit of very large Ω, in which case one finds

$$F_{m,\Omega}(\xi) \approx e^{-\Omega\xi}J_m(2\Omega\sqrt{\xi}), \quad \Omega \gg 1 . \quad (4.33)$$

An illustration of (4.33) is shown in Fig. 13 for the case $m = 2$ and $\Omega = 5$. The tip is shown in two successive positions as it grows in the upward direction; and the time interval has been chosen such that the tip has moved a distance 0.2ρ between the two pictures. (The second stage of the deformation is well beyond the limit of validity of the linear theory.) Note that, because this is the $m = 2$ mode, a section through the dendrite perpendicular to the plane of the paper would show this deformation with the opposite sign; that is, the protuberances would become indentations.

It follows from these results that the Ivantsov needle crystal is manifestly unstable in the absence of capillary forces. There is no upper bound to the spectrum of eigenvalues Ω. According to (4.33), the instabilities are tip-splitting deformations which are localized at the leading edge of the dendrite and which grow more rapidly—Ω increases—as they become sharper and more

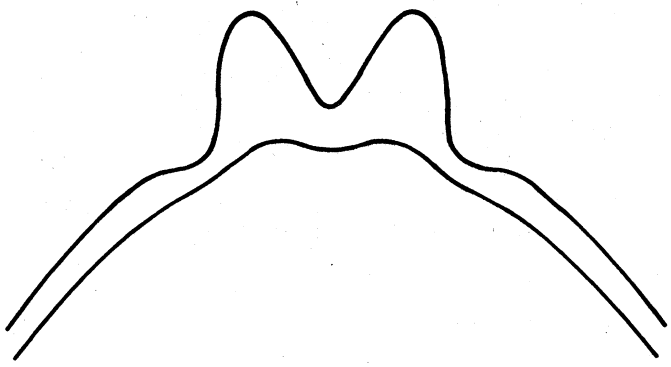

FIG. 13. Unstable tip-splitting mode in the case of vanishing surface tension, computed from Eq. (4.33) with $\Omega = 5$ and $m = 2$. The deformation is shown at two different times; and the time interval is such that the tip has moved upward a distance 0.2ρ between the two pictures.

closely spaced.

To see how the capillary terms in (4.24) restore stability to this system, we have had to resort to numerical techniques. In the computer experiments performed to date, we have looked only at cylindrically symmetric perturbations with $m = 0$; and we have neglected heat flow in the solid, that is, we have dropped the term proportional to σ' in (4.24). The latter omission, plus the neglect of the steady-state shape correction, seriously limits the quantitative validity of these calculations; but it is the qualitative features which are of greatest interest at the moment. We have performed two kinds of numerical experiments. First, we have integrated (4.24) forward in time, either starting with an initial perturbation or applying a persistent random noise at the tip. A more sensitive technique has been to use the ansatz (4.30) and, again, to look for stability eigenstates F_Ω. (That is, we have diagonalized the same finite matrix that was used to approximate the linear-stability operator in the forward-integration method. This is not necessarily equivalent to finding eigenfunctions of the exact operator on the semi-infinite domain $0 \leq \xi \leq \infty$; and it is not even clear that such eigenfunctions exist.) What we find is as follows. For small, finite σ, the tip-splitting deformations occur as before, but they now generate secondary perturbations which move down the dendrite at a speed which keeps them roughly stationary in the laboratory frame of reference. These secondary perturbations grow in amplitude as they move away from the tip; thus the capillary term in (4.24) produces a sidebranching instability. At larger values of σ, the tip stabilizes and there appears to be no eigenvalue Ω with a positive real part; but the sidebranching behavior persists. If one starts with a bump on the dendritic surface near $\xi = 0$, this bump will move down the dendrite leaving an unperturbed paraboloid near the tip. The bump itself will develop into a group of sidebranches growing normal to the main stem of the dendrite at some position which remains fixed in the laboratory frame.

The theoretical sidebranching behavior is illustrated in Fig. 14 for the special case $\sigma = 0.025$, which we believe to be something like the natural operating point for this model of the dendrite. The tip is just marginally stable here, and what is shown is the most active mode, for which $\mathrm{Re}\Omega = 0$, in five successive positions as the dendrite grows up the page. The dashed lines indicate approximate growth paths for the secondary tips. The general features of this figure are encouragingly similar to those of the real succinonitrile dendrite shown in Fig. 12.

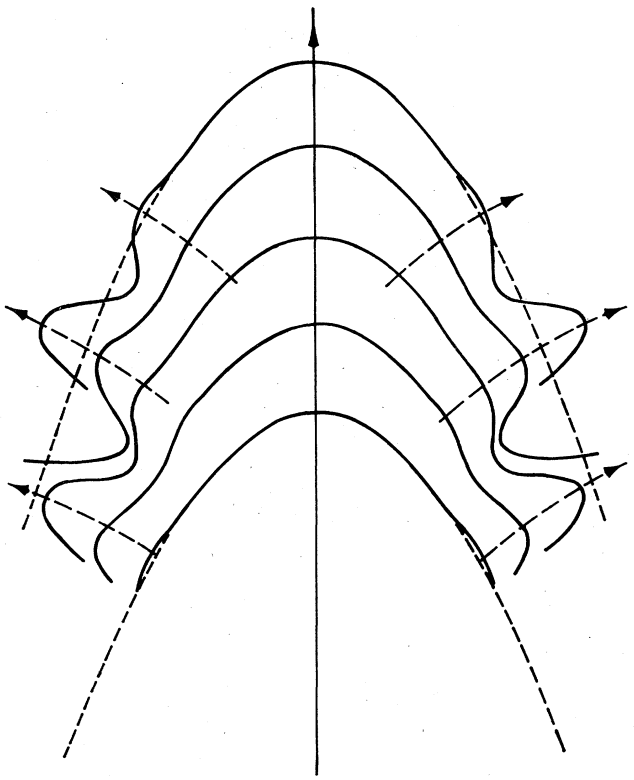

FIG. 14. Dominant sidebranching mode for $\sigma = 0.025$. The tip is shown in five successive positions as the dendrite moves up the page. The dashed lines indicate approximate growth paths for the secondary tips.

C. The marginal-stability hypothesis

At this stage of the discussion, it appears that the linear stability analysis has left us with no new prediction of dendritic growth rates. It would have been nice, for example, if the analysis had shown that there is only one value of σ for which the steady-state system is completely stable. We find, however, that the capillary forces stabilize the tip of the dendrite whenever the dimensionless parameter σ exceeds some critical value. Thus there appears to be a continuous family of relatively sharp, rapidly growing needle crystals, all of which are acceptably stable candidates for the role of main stem of a freely growing dendrite.

Müller-Krumbhaar and I have argued that nonlinear effects must enter the analysis at this point. When a sidebranching deformation attains an appreciable amplitude, it must begin to grow more rapidly outward than inward so that, eventually, the troughs between secondary branches stabilize while the secondary tips continue to grow. The result of this nonlinear behavior must be an effective thickening of the dendrite. The thermal field at the tip will look as if it has been generated by a paraboloidal surface with a larger ρ, which means that v and σ will decrease. Moreover, the sidebranching instability is stronger at smaller velocities; thus a downward fluctuation in velocity will carry the system further toward small σ than an upward fluctuation carries it in the other direction. The net effect, we believe, is that the ever-present sidebranching activity drives dendrites toward slower, fatter configurations—downward and to the right along the steady-state $\tilde{\rho} - V$ curve. If σ becomes too small, however, the dendrite becomes unstable against the tip-splitting deformations described in the previous paragraphs. This suggests that the natural operating point of the dendrite occurs where the tip is just marginally stable. That is, even though dendritic growth appears to be an intrinsically nonlinear process, we hypothesize that the σ^* in

(4.29) can be obtained from a linear stability analysis by finding the minimum σ for which the eigenvalues Ω have no positive real parts.

Unfortunately, it has turned out to be difficult to evaluate σ^* accurately from first principles. In our original numerical analysis, Müller-Krumbhaar and I found σ^* to be in the neighborhood of 0.025, which gave an encouragingly good fit to experiment. However, these calculations assumed cylindrically symmetric deformations and neglected heat flow in the solid. They also omitted the capillarity-related steady-state shape correction, which is probably not serious for the side-branches but may be crucial for a quantitative study of tip stability. All three of these deficiencies are going to require further investigation, especially if we are ever to understand in detail the dynamic behavior of the dendrite tip.

To get a better idea of how the various geometric and kinetic factors may enter into the calculation of σ^*, it is useful to look again at the spherical model of the dendrite tip that was introduced in Eq. (4.10). The stability analysis for the growing sphere was performed in Sec. III.B; and the relevant eigenvalue spectrum is given in Eq. (3.26). If we identify v_R with v and R_0 with ρ, as in the derivation of (4.10), we obtain:

$$\Omega \cong \frac{1}{2}(j-1)[1-\tfrac{1}{2}\sigma j(j+2)(1+\beta+j^{-1})], \tag{4.34}$$

from which we deduce

$$1/\sigma^* = \tfrac{1}{2}j(j+2)(1+\beta+j^{-1}). \tag{4.35}$$

For succinonitrile, β is very nearly unity. (See Glicksman *et al.*, 1976, Table II.) The appropriate value of j is not obvious. The smallest possible choice would be $j=2$, corresponding to a cylindrically symmetric mode with azimuthal index $m=0$, in which the tip becomes sharper or blunter depending on the sign of the deformation. This gives $\sigma^*=0.1$, which is much larger than is observed. On the other hand, if one assumes that only $m=4$ modes are permitted by the cubic anisotropy, as seems to be the case in the experimental photographs, then the lowest possible mode with tip deformation is $j=5$; and $\sigma^*\cong 0.026$. Glicksman's most recent experiments, in which he has made an allowance for convective effects, are in excellent agreement with $\sigma^*=0.0195$, $j\cong 6$ (Glicksman, private communication). But the spherical approximation is much too crude to be taken so seriously. The feature of (4.35) which is likely to remain valid in a more accurate theory is the dependence of σ^* on β, and perhaps some part of its dependence on crystal symmetry via j. It would be very interesting to repeat the measurements of dendritic growth rates for a substance with the same cubic symmetry as succinonitrile but with a thermal conductivity ratio β which is appreciably different from unity, and to see whether σ^* changes as expected.

In the absence of a really reliable, first-principles estimate for σ^*, it seems better to think of the stability hypothesis as a one-parameter theory. As is shown in Fig. 15, the value $\sigma^*\cong 0.025$ predicts growth rates in succinonitrile adequately over two decades in the dimensionless velocity V and one in the undercooling Δ. The theoretical curve in this figure has been drawn by using the simple Ivantsov relation (4.9) for Δ as a function of p, and then evaluating

$$V=\sigma^* p^2. \tag{4.36}$$

A similar comparison can be made for the tip radii, for which case we again use (4.9) plus

$$\tilde{\rho}=1/\sigma^* p. \tag{4.37}$$

Glicksman (private communication) reports that his most recent, convection-corrected measurements of ρ are also in excellent agreement with (4.37) with σ^*

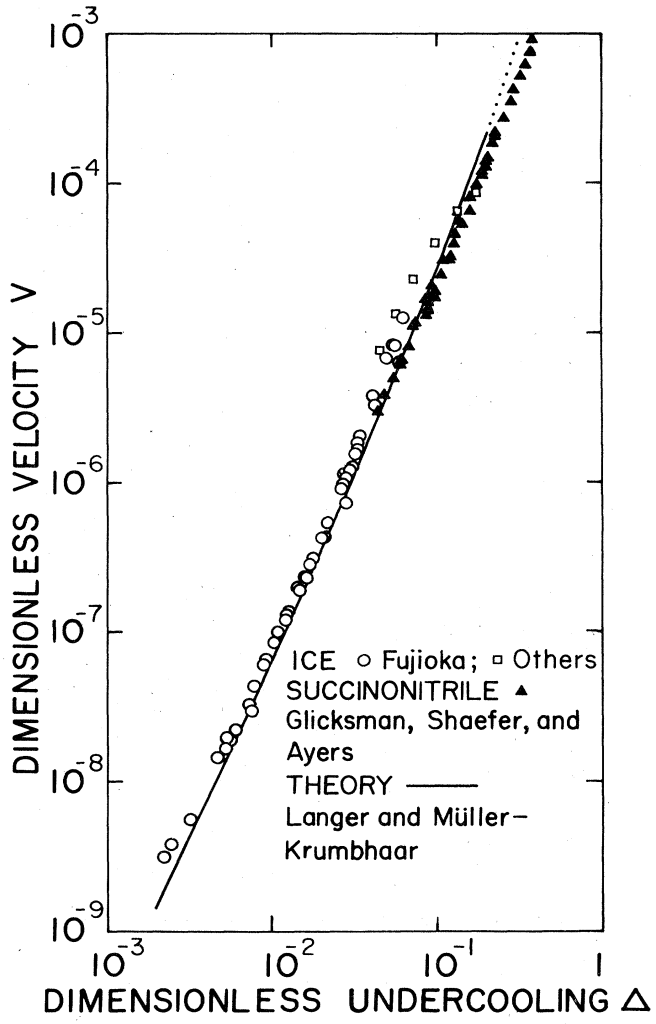

FIG. 15. Dimensionless growth velocity, $V=vd_0/2D$, as a function of dimensionless undercooling $\Delta=(T_M-T)c_p/L$. Experimental points are for ice and succinonitrile as shown. The square points summarize a large body of older data obtained using methods which are not the same as that described in the text, by Lindenmeyer and Chalmers (1966), Hallett (1964), Pruppacher (1967), and Macklin and Ryan (1966, 1968). Omitted from the figure are data at small Δ by Ryan (1969) and by Kallungal and Barduhn (1977). These latter points are scattered, but generally are consistent with Fujioka's results. A composite picture showing all the ice data appears in Sekerka (1976). The theoretical curve is drawn for $\sigma^*=0.025$. The dotted extension to this curve identifies the region where the Péclet number p is greater than 0.1, so that the assumptions leading to Eq. (4.24) may be inaccurate.

$=0.0195$. The overall agreement between theory and experiment, for both V and $\tilde{\rho}$ over a wide range of undercooling Δ, seems to provide strong support for the stability hypothesis.

Surprisingly, Fujioka's data for growth rates of ice dendrites also fit nicely on the $V(\Delta)$ curve in Fig. 15. For ice, β is roughly 4; and the twofold, rather than fourfold, symmetry about the growth axis would seem to require $j=3$ in (4.35). The resulting value of σ^* $\cong 0.025$ seems exactly right; but, in view of the major uncertainties in the theory, I think that this precise agreement must be largely fortuitous. It seems to me that the present form of the theory cannot be adequate to describe so highly anisotropic a system, and that, in particular, anisotropic attachment kinetics must be included in both the steady-state calculation and the stability analysis.

Despite its apparent success in the interpretation of experimental results, the stability theory of dendritic growth is fundamentally incomplete. The stable operating point of a dendrite seems to be a complex, dynamic, essentially nonlinear state of the system; and I must emphasize that we do not understand this state at all yet. We have no satisfactory model of the mechanism by which the tip instability at $\sigma<\sigma^*$ restores σ to the neighborhood of σ^* without destroying the dendritic structure. Presumably, there exists some higher-order coupling between the unstable modes and the steady-state parameters ρ and v. This coupling might cause the system to move in some sort of stable limit cycle in which ρ and v oscillate, and in which the frequency and amplitude of the oscillation are completely fixed by nonlinear extensions of the deterministic equations of motion derived above. On the other hand, the motion might be irregular, perhaps some sort of Brownian motion driven by thermal fluctuations. Until we understand this point, we shall not know whether the stability criterion is exact, or is just an approximation with a limited range of validity, or really whether it makes any sense at all. Nor shall we know how to compute a number of interesting quantities, most particularly, the amplitudes and ultimate spacings of the sidebranches.

We have not made much progress in analyzing the dendritic operating point along the lines suggested above. The difficulty, I think, is a clue to answering the question raised in the Introduction regarding sensitivity to growth conditions and material parameters. Our hypothetical operating point is marginally unstable against three independent and nontrivial modes of deformation. First, of course, is the dominant tip-splitting or sharpening mode whose neutral stability point occurs just at $\sigma=\sigma^*$. In addition, there is the simple translation along the growth axis; and, because we have insisted that our basic paraboloid be a steady-state solution of the equations of motion, there always must be a third marginally unstable mode in which ρ and v shift together along the steady-state ρ-v curve. This simultaneous occurrence of three modes of deformation for which the linear restoring force vanishes produces an extremely delicate nonlinear situation in which detailed behavior is controlled by relatively small, higher-order terms in the equations of motion. These terms are difficult to evaluate. In principle, however, this delicacy is exactly what we need in order to understand the apparent sensitivity of pattern forming processes. The sidebranches must be initiated by microscopic thermal fluctuations near the tip of the dendrite; but they never fail to occur and to play a dominant role in the dendritic growth process. If their amplitudes are controlled by small, nonlinear terms, then it is plausible that these amplitudes, and also the orientations and shapes of the sidebranches, will be sensitive to small changes in temperature or small anistropies in molecular attachment coefficients.

V. CELLULAR INTERFACES

A. The one-sided model

Because of the special simplicity of its planar geometry, the problem of directional solidification provides a good opportunity for carrying out in detail a fully nonlinear analysis. The purpose of such an analysis is to follow the development of an initially unstable perturbation and to understand the actual mechanism by which new patterns are formed. In the planar situation, a limited version of the problem can systematically be reduced to a set of coupled nonlinear equations involving only a finite number of degrees of freedom. Specifically, we can assume that the interfacial displacement ζ, as defined in (2.13), is always strictly periodic in, say, the x direction. Then

$$\zeta(x,t)=\sum_n A_n(t)\exp(ink_1x)\,, \tag{5.1}$$

where k_1 is the fundamental wave number and, without loss of generality, we may assume the amplitudes A_n to be real and to satisfy $A_{-n}=A_n$. In a quasistationary approximation, the A_n will satisfy equations of motion of the form

$$dA_n/dt=\Phi^{(n)}\{A\}\,, \tag{5.2}$$

where each of the $\Phi^{(n)}$ is in principle a function of all the A's. If the Fourier series (5.1) can be approximated by a small number of terms, then the system of equations (5.2) can be studied numerically. Furthermore, if the fundamental amplitude A_1 can be assumed to be small—for example, for short times after the onset of instability or for nearly critical growth conditions—then the right-hand side of (5.2) can systematically be expanded in powers of A_1. Research along these lines has been carried out for many years in connection with the hydrodynamic instabilities (Segel, 1966), especially the Bénard problem where the planar geometry permits Fourier analysis as in (5.1); but the analogous solidification problem has remained relatively unexplored. In what follows, I shall summarize recent developments in this area, my main purpose being to direct attention to some promising lines of investigation.

Before plunging into nonlinear analysis, it is important to choose some particular model and to adopt appropriate descriptive parameters. We shall consider two such models in this chapter: first, a realistic but mathematically difficult one and, second, an idealized but slightly more tractable system. The model for which there is a better chance of finding experimental comparisons is what I shall call the "one-sided" model. The

basic features of this system are:

(a) Latent heat is negligible.

(b) Thermal conductivities are the same in both liquid and solid phases; $c_p D_T = c_p' D_T'$.

(c) The chemical diffusivity vanishes in the solid; $D_c' = 0$.

Assumptions (a) and (b) already were built into the analyses of Secs. II.C and III.C. Remember that it was this pair of assumptions which permitted us to use a constant thermal gradient G and thus to decouple the thermal field from the motion of the interface. Point (c) is new, but is quite accurate for dilute alloys—probably more accurate than (b). Given all three assumptions, we are left with only three characteristic lengths in the problem: the chemical diffusion length $l = 2D_c/v$, the thermal length l_T defined in (3.33), and the capillary length d_0 defined in (3.5). Any pair of ratios of these lengths will serve as a complete set of dimensionless system parameters. We already have introduced $\nu = 2l_T/l$ in (3.37), and have concluded that the interesting values of this parameter are of order unity. Of the ratios involving d_0, we choose d_0/l, and note that this quantity is the same dimensionless group of parameters that we denoted by V in Sec. IV.

The most detailed study of the one-sided model, and probably the most comprehensive piece of work in this field to date, is that of Wollkind and Segel (1970). These authors do not adopt assumption (b) but, rather, keep the thermal diffusion fields on both sides of the interface as space- and time-dependent quantities. They also do not explicitly make a quasistationary approximation for the chemical diffusion field. The resulting analysis is exceedingly complicated, but has the potential advantage of being directly comparable with experiment.

To understand the nature of the Wollkind–Segel results, it is necessary first to go back to the linear-stability result (3.31). For the one-sided case, we can write the exact version of this equation in the form:

$$\frac{\omega l^2}{2D} = (ql - 2 + 2K)\left[1 - \frac{1}{\nu} - \frac{1}{2} V(kl)^2 - \frac{2K}{ql - 2 + 2K}\right], \tag{5.3}$$

where

$$ql = 1 + \sqrt{1 + (kl)^2}\,, \tag{5.4}$$

and $V = d_0/l$. In writing (5.3), we have made the additional assumption that the ratio μ_c/μ_c', defined in (3.32), is identical to the partition coefficient K. This assumption seems to be common in the metallurgical literature. The right-hand side of (5.3) is sketched in Fig. 16 as a function of kl for fixed V and several different values of ν. (Think of keeping the velocity v constant and varying the stability parameter ν by changing the temperature gradient G or the impurity concentration.)

The quantity in square brackets in (5.3) passes through a maximum as a function of k. In the limit of very small V, this maximum occurs at large k, spec-

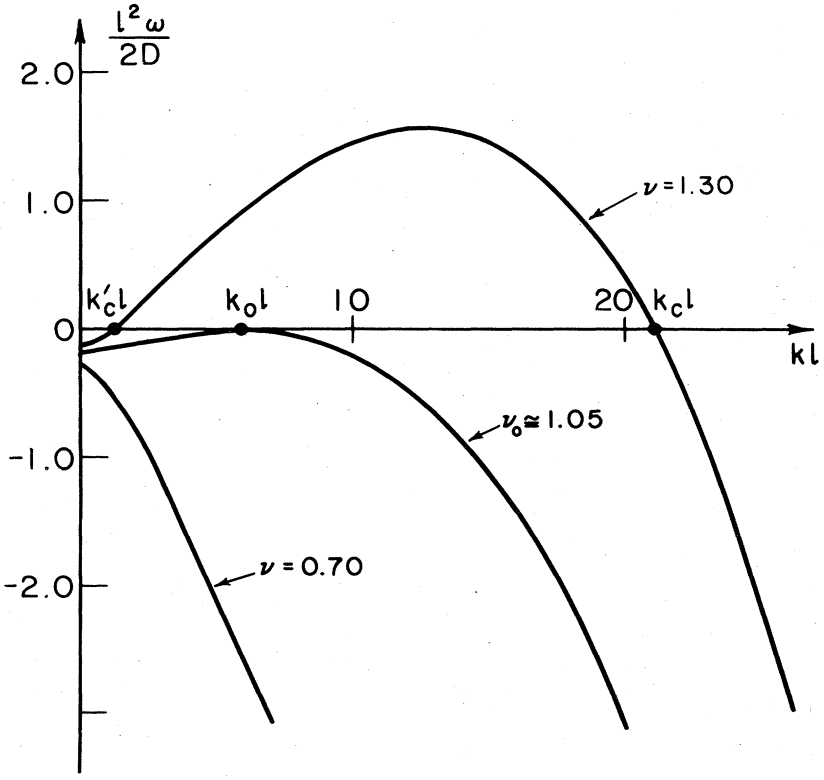

FIG. 16. Amplification rate ω for the one-sided model, as a function of wave number k, for $V = 0.001$, $K = 0.1$, and for three values of ν as shown.

ifically, $k = k_0$ where

$$k_0 l \cong (2K/V)^{1/3}; \quad V \ll 1. \tag{5.5}$$

The critical value of ν, which we denote by ν_0, occurs when this maximum passes through $\omega = 0$; thus[5]

$$\nu_0 \cong 1 + 3(K^2 V/2)^{1/3}; \quad V \ll 1. \tag{5.6}$$

For values of ν less than ν_0, the plane is stable against infinitesimal deformations of all wavelengths. For ν greater than ν_0, however, there is a band of unstable deformations with wave numbers k between k_c' and k_c, as shown in Fig. 16. Equation (5.6) illustrates, for a specific model, the way in which capillary and kinetic effects induce deviations from the simple rule of constitutional supercooling.

The nonlinear analysis presented by Wollkind and Segel is of a special kind which is not easily generalized to large-amplitude deformations, but which gives very interesting information for near-critical growth conditions, that is, for $\nu \cong \nu_0$. The calculation starts, in effect, with an expansion of the functions $\Phi^{(n)}$ in (5.2) in powers of the amplitudes A_n. The principal step in the analysis is the construction of a formal solution of (5.2) in terms of a single time-dependent function which I shall denote, for simplicity, by $\varepsilon(t)$. It turns out—and we shall see this more explicity below in connection with the symmetric model—that if A_1 is small of order ε, then there is a solution of (5.2) in which A_2 is of order ε^2, A_3 of order ε^3, etc. More precisely, A_1 can be expressed as a series in odd powers of ε starting at ε^1; A_2 as a series in even powers starting at ε^2, etc. The function ε satisfies an equation of the form

$$d\varepsilon/dt = a_0 \varepsilon - a_1 \varepsilon^3 + \cdots, \tag{5.7}$$

where a_0 is the linear stability parameter:

$$a_0 = \omega(k_1). \tag{5.8}$$

The crux of the Wollkind–Segel paper is the calculation of the Landau constant a_1. Strictly speaking, both a_0 and a_1 are functions of k_1 as well as ν and V. By definition, a_0 changes sign as one moves from stable to unstable conditions; but a_1 might be reasonably constant in the transition region. Thus Wollkind and Segel evaluate a_1 at the neutral stability point, $\nu = \nu_0$, $k_1 = k_0$, for different values of V. Positive values of a_1 are taken to indicate the possibility of a restabilized cellular interface with, according to (5.7), $\varepsilon^2 \cong a_0/a_1$. Choosing a partition coefficient $K = 0.2$, they find that a_1 is positive only for values of V larger than about 0.3, which corresponds to values of $k_0 l$ (their ω_c) smaller than about 0.5. This regime of parameter values is awkward theoretically because, as we have seen at the end of Sec. III.A, the quasistationary approximation is invalid at such small values of k_0. To achieve this situation experimentally, one must arrange that the capillary length d_0 be large and comparable to l, so that V is large. This can be accomplished by working with very dilute solutions [see Eq. (3.5)]; and, indeed, cellular solidification fronts have been observed in very dilute metallic alloys under roughly the conditions described here.

For appreciable solute concentrations, d_0 becomes microscopically small, and the nonlinear analysis for the one-sided model seems to indicate that an interface will make a direct transition to some kind of dendritic or otherwise non-steady-state behavior upon the onset of instability. It is possible that stable cellular solutions exist, but that they are beyond the range of the small-amplitude approximation. This seems unlikely, however, in view of the results to be described in the paragraphs which follow.

B. The symmetric model

The one-sided model possesses several mathematical complexities which make it difficult—but, I think, not impossible—to extend a nonlinear analysis beyond the first terms shown in Eq. (5.7). The basic difficulty is that the diffusion law itself—not just the diffusion field—is discontinuous across the two-phase interface. As a result, the diffusion field is perturbed by the interface whether or not the interface is playing any kinetic role in the process, i.e., generating latent heat or rejecting impurities. To achieve a more tractable situation, Turski and I have introduced what we call the "symmetric model" (Langer and Turski, 1977; Langer, 1977). The thermal properties of this model are the same as those of the one-sided model; that is, there is a fixed temperature gradient, and points (a) and (b) in Sec. V.A remain unchanged. Instead of (c), however, we assume:

(c′) Chemical diffusion is identical in the two phases; $D_c' = D_c$; $M' = M$; $\beta = 1$; and we further specify that:

(d′) The miscibility gap ΔC is independent of temperature; $K = \mu_c/\mu_c' = 1$. These new assumptions are unrealistic for solidification problems; but the model retains most of the qualitative features of interest here, and it may also provide a useful description of nonequilibrium interfaces in certain liquid–liquid or solid–solid systems.

We now need only a single diffusion field u to describe the entire two-phase system:

$$u = \delta C/\Delta C, \tag{5.9}$$

where δC represents the difference between the local concentration and its phase-dependent equilibrium value at the reference temperature T_0. [See Eqs. (2.11) and (3.1) and Fig. 6]. The field u satisfies the diffusion equation with $D = D_c$ everywhere, and obeys the boundary condition $u \to -1$ infinitely far ahead of the advancing solidification front. The interface very simply plays the role of a distributed source for this field, the source strength per unit area being proportional to the normal velocity of the surface. The general equation of motion for this interface can be obtained as follows. Let $\mathcal{G}$ be the Green's function for diffusion in a frame of reference moving in the z direction with velocity v:

[5] Equation (5.6) describes the small-V portion of the neutral-stability curve for this system. The corresponding curve in Wollkind and Segel (1970) is shown in their Fig. 4, where their G is essentially the same as our $1/\nu_0$, and their γ is proportional to our V. Their curve is drawn incorrectly at small V but this graphic error does not affect the validity of their analysis.

$$\mathcal{G}(\mathbf{x},z,t)=\frac{1}{(4\pi Dt)^{3/2}}\exp\left[-\frac{x^2+(z+vt)^2}{4Dt}\right]. \tag{5.10}$$

Note that $\mathcal{G}$ describes the field at $(\mathbf{x},z,t)$ arising from a point source at the origin, and that $\mathcal{G}$ vanishes at infinity. Integrating over the source distribution on the interface, and assuming that there are no other sources or perturbations in the system, we find the field at any point $(\mathbf{x},z,t)$ to be

$$u(\mathbf{x},z,t)=-1+\int_{-\infty}^{t}dt'\int d^2x'\,\mathcal{G}(\mathbf{x}-\mathbf{x}',z-\zeta',t-t')\left(v+\frac{d\zeta'}{dt'}\right), \tag{5.11}$$

where ζ' denotes $\zeta(\mathbf{x}',t')$. This expression is well defined everywhere, even for points on the interface where $z=\zeta(\mathbf{x},t)$. At such points, u must satisfy the thermodynamic boundary condition deduced from (2.16), (3.1), and the symmetry assumptions (c',d');

$$u(\text{Interface})=u(\mathbf{x},\zeta,t)=-d_0\mathcal{K}\{\zeta\}-(1/l_T)\zeta. \tag{5.12}$$

Combining (5.11) and (5.12), we obtain

$$d_0\mathcal{K}\{\zeta\}+\frac{1}{l_T}\zeta(\mathbf{x},t)+\int_{-\infty}^{t}dt'\int d^2x'\,\mathcal{G}(\mathbf{x}-\mathbf{x}',\zeta-\zeta',t-t')\times\left(v+\frac{d\zeta'}{dt'}\right)-1=0. \tag{5.13}$$

This is a nonlinear integrodifferential equation[6] for $\zeta(\mathbf{x},t)$.

The memory effect shows up clearly in (5.13); in order to compute the interfacial velocity at time t, we must know the history of the interface at all earlier times t'. This is not a major difficulty for linear-stability analysis; but we shall find it very useful to go directly to a quasistationary approximation for purposes of the nonlinear theory. The conditions for the validity of this approximation remain as described in Sec. III.A. As applied to (2.13), the approximation requires that ζ vary so slowly in time that we can replace $\zeta(\mathbf{x}',t')$ by $\zeta(\mathbf{x}',t)$ everywhere inside the integrand. The remaining integration over t' can be performed explicitly. If we then insert the Fourier expansion for ζ, Eq. (5.1), we obtain from (5.13) a set of coupled, nonlinear equations of the form:

$$\sum_{n'}\Gamma_{n,n'}\{A\}\frac{dA_{n'}}{dt}=\tilde{\Phi}^{(n)}\{A\}, \tag{5.14}$$

where the matrix Γ is computed in an obvious way from $\mathcal{G}$. Γ is nonsingular and can, in principle, be inverted so as to write (5.14) in the form of (5.2).

Let us look first at a small-amplitude expansion of (5.14) analogous to the method used by Wollkind and Segel. If ζ vanishes, the Green's function $\mathcal{G}$ recovers translational symmetry, and the matrix Γ is diagonal. The leading nonlinearities occur in the expansion of $\tilde{\Phi}^{(n)}$ on the right-hand side. The first two equations have the form

$$\Gamma_{11}(dA_1/dt)+\cdots=\tilde{\Phi}_1^{(1)}A_1+\tilde{\Phi}_2^{(1)}A_1A_2+\Phi_3^{(1)}A_1^3+\cdots \tag{5.15}$$

$$\Gamma_{22}(dA_2/dt)+\cdots=\tilde{\Phi}_1^{(2)}A_2+\tilde{\Phi}_2^{(2)}A_1^2+\cdots. \tag{5.16}$$

More generally,

$$\Gamma_{n,n}(dA_n/dt)+\cdots=\tilde{\Phi}_1^{(n)}A_n+\Phi_n^{(n)}A_1^n+\cdots. \tag{5.17}$$

The rule for writing higher-order terms on the right-hand side is that, in any product of terms $A_{|k|}A_{|l|}A_{|m|}\cdots$ appearing in the nth equation, $k+l+m+\cdots$ must equal n. The Fourier indices k,l,m can have either sign, but we continue to use $A_{-n}=A_n$. Because of the symmetry of the model, the mode $n=0$ does not appear here.

The first-order terms in these equations reproduce the results of the quasistationary linear-stability theory. Specifically,

$$\tilde{\Phi}_1^{(n)}/\Gamma_{n,n}=\omega(nk_1), \tag{5.18}$$

where

$$\frac{l^2\omega(k)}{2D}=\sqrt{1+(kl)^2}\left[1-\frac{1}{\nu}-V(kl)^2-\frac{1}{\sqrt{1+(kl)^2}}\right]. \tag{5.19}$$

Equation (5.19) may be obtained either directly by expansion of (5.13) or by setting $\beta=\mu_c/\mu_c'=K=1$ in the general first-order formula (3.36). In writing this last result, we have used the same definitions of l and V as in the previous sections, and have used $\nu=l_T/l$ as required by (3.37). The higher-order coefficients in (5.15) through (5.17) are obtained by expanding the $\tilde{\Phi}$'s in powers of the A's. Specific formulas for these coefficients may be found in Langer (1977).

The Wollkind-Segel analysis is valid when ν and k_1 are very near their critical values, ν_0 and k_0, so that $\omega(k_1)$ just vanishes at $k_1=k_0$ and is negative elsewhere. For the symmetric case (5.19), and very small V, we have

$$\nu_0\cong 1+\tfrac{3}{2}(2V)^{1/3};\quad k_0l\cong\left(\frac{1}{2V}\right)^{1/3}V\ll 1. \tag{5.20}$$

The near-vanishing of $\omega(k_1)$ means that $\omega(2k_1)<0$, and thus the mode A_2 is stable. According to (5.16), A_2 relaxes to a value of order A_1^2 at a rate $\omega(2k_1)$ which is fast compared to the rate $\omega(k_1)$ at which A_1 is varying. Similarly, higher-order amplitudes A_n relax even more rapidly to values of order A_1^n. Equation (5.7) effectively picks out a special formal solution of the equations of motion in which there are no initial transients in the higher modes and the process is dominated by the slow mode A_1. Under these circumstances, there is nothing to be lost by simply setting the left-hand side of (5.16) equal to zero, solving for A_2, and then rewriting (5.15) as an equation of motion for A_1. The result is similar to (5.7):

$$dA_1/dt\cong\omega(k_1)A_1-a_1A_1^3+\cdots, \tag{5.21}$$

where the Landau constant turns out to be:

$$a_1=\frac{1}{\Gamma_{11}}\left(\frac{\tilde{\Phi}_2^{(1)}\tilde{\Phi}_2^{(2)}}{\tilde{\Phi}_1^{(2)}}-\tilde{\Phi}_3^{(1)}\right)\cong\frac{2D}{Vl^4}\quad(\nu=\nu_0;k_1=k_0;V\ll 1). \tag{5.22}$$

In contrast to the one-sided model, the Landau constant a_1 given by (5.22) is always positive, at least for small V. This means that, under just slightly supercritical conditions, $\nu\gtrsim\nu_0$, the symmetric model may

[6] Similar, more general, integral-equation methods have been used for problems of this kind by Nash (1974) and by Strässler and Schneider (1974).

form restabilized cellular interfaces with wave numbers k_1 near k_0. These cellular structures have stationary amplitudes A_{1s}:

$$A_{1s}=[\omega(k_1)/a_1]^{1/2}; \tag{5.23}$$

and (5.21) can be recast in the form

$$\frac{d}{dt}(A_1-A_{1s})=-2\omega(k_1)(A_1-A_{1s})+\cdots, \tag{5.24}$$

which implies cellular stability for positive $\omega(k_1)$. Thus within this single-mode, small-amplitude approximation, there exists a stable, nonplanar, stationary interface at any wave number k_1 for which the plane itself is unstable.

Studies of the symmetric model have been carried beyond this point in two general directions. First, we have performed a more complete stability analysis of the small-amplitude cellular structures which are stationary solutions of (5.21). The second extension is a search for finite-amplitude steady-state solutions at larger values of ν. Much of this work is described in the 1977 paper; but some portions of the material to be presented below are new.

The general stability problem arises because the equations of motion (5.2) or (5.14) describe only very special deformations of the interface, specifically, those which preserve a fundamental periodicity k_1. A complete analysis must test the interface for stability against all possible smooth, infinitesimal deformations, including those which tend to change the periodicity. To perform this analysis, we can write the general interfacial displacement $\zeta(\mathbf{x},t)$ in the form

$$\zeta(\mathbf{x},t)=\zeta_s(\mathbf{x})+f(\mathbf{x})\exp(\tilde{\omega}t), \tag{5.25}$$

where $\zeta_s(\mathbf{x})$ is the stationary cellular solution, and f is an infinitesimal deformation. The equation of motion, (5.13), can then be linearized in f. If we make a quasistationary approximation, the resulting eigenvalue equation for $\tilde{\omega}$ has most of the properties of a Schrödinger equation for a particle moving in a periodic potential of wave number k_1. In particular, one can define a Bloch wave number κ, and can compute bands N of eigenvalues $\tilde{\omega}_N(k_1,\kappa)$ for values of κ in the "Brillouin zone", $-k_1/2\leq\kappa\leq k_1/2$. Stability requires that no $\tilde{\omega}$, for any κ in any band, be greater than zero.

For the small-amplitude states where the in-phase deformations, i.e., those described by (5.24), are stable, the most dangerous modes turn out to be those associated with sidewise translations of the cellular pattern. An infinitesimal translation, for which f in (5.25) is proportional to $d\zeta_s/dx$, must have a vanishing relaxation rate $\tilde{\omega}$. Such a mode is not accessible to our previous analysis because it must be described by a Fourier series whose coefficients are antisymmetric, $A_{-n}=-A_n$. We further argue that this translation mode must correspond to a state with $\kappa=0$ in a band of deformations which cause shifts in the fundamental periodicity of the original cellular pattern. To see this, suppose that, for small but nonzero κ, the mode shifts the cells near $x=0$ slightly to the right. The same shift will recur at positions along the x axis separated by the Bloch wavelength $2\pi/\kappa$, which we may imagine to be much larger than the underlying cellular spacing $2\pi/k_1$. In between these positions, the cells are shifted to the left; and, at the $\frac{1}{4}$- and $\frac{3}{4}$-Bloch wavelength positions, respectively, they are compressed and expanded. If the system is unstable against compression or expansion of the cells, the amplitude of such a mode will grow exponentially.

To determine whether this sort of deformation is stable, we need simply examine the translation band, denoted by $N=0$, in the neighborhood of $\kappa=0$. By symmetry, we must have

$$\tilde{\omega}_0(k_1,\kappa)\cong\frac{1}{2}\mathfrak{D}_0(k_1)\kappa^2+\cdots. \tag{5.26}$$

Negative values of $\mathfrak{D}_0(k_1)$ can be taken to imply differential stability of the cellular structure with wave number k_1. A detailed calculation of $\mathfrak{D}_0(k_1)$ is reported in the 1977 paper for a fixed value of ν. The calculation indicated that there exists a finite range of values of k_1 for which the cells are stable.

It is useful to recast the results of the above stability calculation in terms of the dimensionless control parameters introduced in this review. Consider a very small, fixed value of the dimensionless velocity V. If we set to zero the quantity in square brackets in the formula (5.19) for $\omega(k)$, we obtain a function $\nu_c(k)$ which, for very slightly supercritical ν_c, can be written in the form

$$\nu_c(k)\cong\nu_0+3Vl^2(k-k_0)^2+\cdots. \tag{5.27}$$

Here, ν_0 and k_0 are the critical values of ν and k given by (5.20). The exact function $\nu_c(k)$ is indicated by the solid curve in Fig. 17. The parabolic minimum of this curve is given by (5.27). At a given ν, points k inside this curve ($k_c'<k<k_c$) indicate wave numbers at which the planar interface is unstable, and at which stationary—but not necessarily fully stable—cellular interfaces will occur with fundamental wave numbers $k_1=k$. The locus of points at which $\mathfrak{D}_0(k)$ vanishes turns out to be

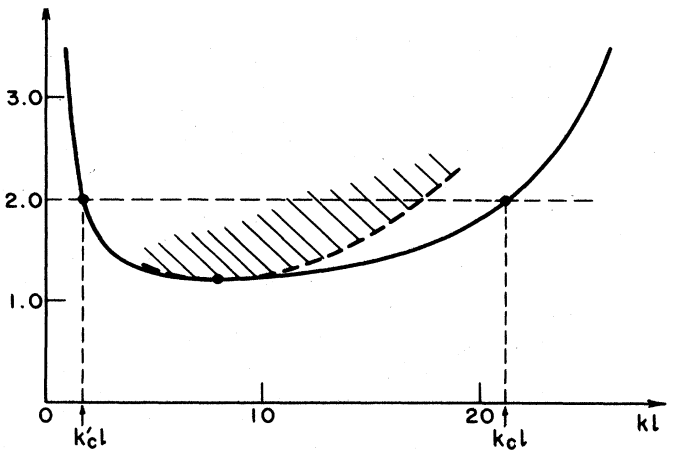

FIG. 17. Regions of stability in the ν-k plane for the symmetric model with $V=0.001$. The planar interface is stable at points outside, i.e. below, the solid curve. Small-amplitude cellular interfaces are differentially stable (against longitudinal deformations) in the shaded region above the dashed parabola. It is not known what happens to this region at large values of ν. Values of k_c and k_c' are shown for the special case $\nu=2$.

given by a similar relation:

$$\nu_D(k) \cong \nu_0 + 9Vl^2(k-k_0)^2 + \cdots , \tag{5.28}$$

which is indicated by the dashed parabola in Fig. 17. Points in the shaded region inside the latter parabola locate cellular states which have complete differential stability.[7]

Note that we have arrived at a situation which is reminiscent of the dendrite problem. The most we can do experimentally is to fix V and ν; and the system itself must then determine its interfacial configuration, including the wave number k_1. Just as in the dendrite problem, however, our mathematics has produced a whole family of linearly stable steady-state solutions. Unfortunately, the experimental situation here is not so clear as it was for the dendrites; we do not know yet whether nature has a strong preference for just one of these states. The analog of the dendritic situation would be a nonlinear mechanism tending to drive the system toward the left or right boundary of the stable shaded region, at which point the system would be marginally unstable and would, perhaps, undergo some sort of limit cycle. Alternatively, the system might retain whatever periodicity formed most rapidly after the onset of planar instability; or the periodicity might always be determined by boundary effects. As far as I know, there exist no theoretical or experimental reasons for favoring any of these hypotheses.

Let us turn, finally, to the question of what happens at strongly supercritical values of the control parameters. Very little is known with any certainty in this area, but one important qualitative conclusion seems to be emerging from the work done so far: the picture of smooth, stationary, restabilized cellular interfaces seems to break down outside of a rather narrow range of values of the control parameter ν. We have tried two different mathematical approaches to this problem. First, as described in the 1977 paper, we have looked at an approximation that ought to be valid when both the fundamental mode at wave number k_1 and the first harmonic at $2k_1$ are simultaneously unstable. The second approach is a direct numerical search for stationary solutions of the integral equation (5.13). The numerical approach, which will not be described here in any detail, has served to check the accuracy of the expansion method and to extend the cellular calculations somewhat beyond the point where the expansion method breaks down.

Most of the important results of these calculations are summarized in Figs. 18 and 19. These figures actually have been obtained by the numerical method for the case $\nu = 1.40$, which is just beyond the apparent range of the expansion technique; but the higher-order expansion also produces the qualitative features illustrated here. Figure 18 shows the root-mean-square amplitude of a cellular interface:

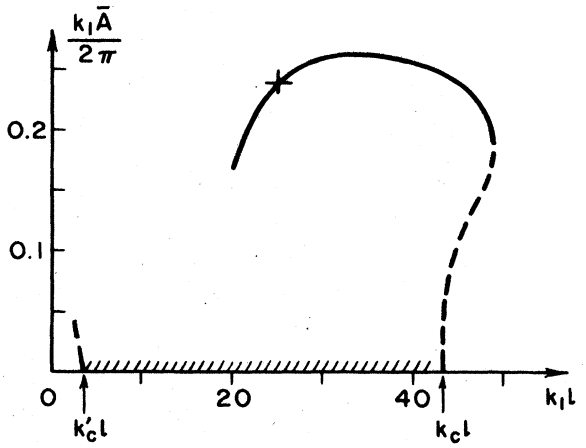

FIG. 18. Root-mean-square amplitude of cellular interfaces, $\bar{A}$, as a function of fundamental wave number k_1, for the symmetric model with $V = 1.4 \times 10^{-4}$, $\nu = 1.4$.

$$\bar{A} = \left[2\sum_{n=1}^{\infty} A_n^2\right]^{1/2} , \tag{5.29}$$

in units of the wavelength $2\pi/k_1$, as a function of the fundamental wave number k_1. The shaded region along the k_1 axis indicates the range of wave numbers between k_c' and k_c where the planar interface is unstable. The solid curve shows values of $\bar{A}$ for cellular interfaces which are stable against wavelength-conserving perturbations, that is, which are stable against small variations of the amplitudes A_n. The dashed lines describe stationary solutions which are manifestly unstable. (It is not known whether any of these solutions possess complete differential stability.) The interfacial profile $\zeta_s(x)$ illustrated in Fig. 19 has parameters k_1, $\bar{A}$ indicated by the point X in Fig. 18.

A variety of interesting things have happened in Fig. 18. Note that the point k_c—the maximum k at which the planar interface is unstable—is a bifurcation point for the planar and cellular stationary solutions, and that it makes sense to use a small-amplitude expansion to study these solutions near this point. However, the Landau constant a_1 defined in (5.21) and (5.22) but evaluated at $\nu = 1.4$, $k_1 = k_c$ has become negative. Accordingly, the small-amplitude stationary states occur with $k_1 > k_c$ and are unstable. [See (5.24) and note that $\omega(k_1) < 0$ in this case.] The possibly stable cellular states all have relatively large amplitudes and occur with wave numbers k_1 in a range which extends beyond k_c. If the interface is to make a direct transition to a

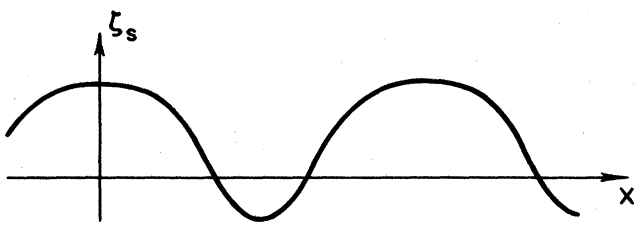

FIG. 19. Cellular interface corresponding to the point labeled X in Fig. 18.

[7]For a different but closely related analysis of the stability of Bénard convection patterns, see Newell and Whitehead (1969). In comparing the two results, remember that here we have considered only longitudinal deformations (expansions and compressions) of the cells, whereas Newell and Whitehead have included transverse deformations of their rolls.

state at $k_1 > k_c$ without undergoing a change in periodicity, it must start with a finite rather than an infinitesimal deformation. The small-amplitude states near the lower bifurcation point k_c' also are strongly unstable. At wave numbers just above k_c', there seem to exist no stationary cellular solutions at all. The smallest wave number at which cellular solutions appear is roughly equal to the smallest k_1 for which the first harmonic $2k_1$ is stable. In other words, the bottom of the band of stationary solutions is approximately $k_c/2$.

The interfacial profile shown in Fig. 19 exhibits the symptoms, if not the fully developed features, of the cellular structure shown in Fig. 7. The leading edges are relatively flat and the groove-roots are sharply curved. The pattern is shifted forward so that most of the interface is warmer than the reference temperature T_0 and the solute is concentrated in the cooler, narrow grooves.

Our attempts to extend the numerical calculations much beyond $\nu = 1.40$ have so far been unsuccessful, and the breakdown of the calculation occurs in a way which suggests that there may not exist truly stationary, finite, and stable cellular structures in that regime. At $\nu = 1.50$, the smooth solid curve which locates stable solutions in Figure 18 seems to twist and break up into pieces; and none of these apparent solutions seems to be either physically plausible or numerically reliable. Both the numerical evidence and the observations described in Sec. II.C and illustrated in Fig. 7 suggest that the stationary solution breaks down in the grooves.

It would be very useful if we could somehow avoid having to perform a completely time-dependent computation in order to analyze these large-scale cellular structures. One possibility is that the mathematical grooves might actually become infinitely deep and sharp, as shown in Fig. 7, and that the thermodynamic boundary conditions can be relaxed at the isolated points of infinite curvature. Unfortunately, this relatively simple picture cannot be exactly correct at any finite value of ν. Deep inside the grooves, where the interfaces are parallel to the direction of growth, there are no nearby sources for the diffusion field and (5.13) must reduce to

$$d_0 \mathcal{K}(\xi) \approx -\frac{1}{\nu l}\,\zeta(x)\,. \tag{5.30}$$

Thus, if ζ becomes large and negative, the curvature must become appreciable; and this is inconsistent with our original picture. One way out of this difficulty is to let ν become infinitely large, that is, to look first at the limit of vanishingly small thermal gradient. If well-behaved stationary solutions exist in this limit, then one might guess that, for large but finite ν, these solutions would remain accurate for the frontmost portions of the cells, and that nonstationary behavior might occur at a distance down the grooves determined roughly by setting the curvature on the left-hand side of (5.30) equal to the inverse cell spacing. It turns out that these infinitely elongated cellular solutions can be found numerically. They seem to occur within a rather narrow band of wave numbers k_1 in the neighborhood of $2k_s$, where $k_s l \cong V^{-1/2}$ is the inverse stability length originally defined in Eq. (3.15). Note that the spacing of these cells is smaller than the smallest wavelength for which the plane is unstable. Figure 7 is actually a computed cellular structure, obtained by a numerical procedure based on the stationary version of (5.13) with $\nu = \infty$, $V = 0.004$.

VI. SUMMARY: OUTSTANDING PROBLEMS

Throughout this essay, and especially in the last two sections, we have encountered a wide variety of unsolved problems in solidification theory. The best way to summarize this paper as a whole may be simply to list the most interesting of these unsolved problems. We then may try to gauge present progress and future opportunities by the extent to which we can pose pointed and sensible questions.

Let us start with questions pertaining to dendrites. The sidebranching mechanism and the marginal-stability hypothesis have provided us with a new starting point for both theoretical and experimental investigation. However:

(1) We have no firm theoretical basis for the marginal-stability hypothesis. Is it correct? If so, what actually happens in the nonlinear operating mode of the dendrite? Does the system undergo a limit cycle? What role is played by thermal fluctuations?

(2) We have no reliable and systematic means for evaluating the stability parameter σ^*. Part of the problem is in the numerical analysis. How does one obtain accurate solutions to a non-Hermitean stability problem, Eq. (4.24), for a semi-infinite system $(0 \leq \xi < \infty)$ in which the most interesting deformations—the sidebranches—grow without bound at large ξ? Does the spherical approximation have any validity? How important are capillary corrections to the steady-state solution?

These are the most basic and immediate theoretical problems. Questions of more practical interest include:

(3) What is the effect of crystalline anistropy? How does one include anisotropic attachment kinetics in the steady-state problem or in the stability analysis? Can one construct a quantitative theory for a strongly anistropic system such as, say, ice?

(4) What role do impurities play in dendritic growth? There is some evidence (Lindenmeyer, 1959; Fujioka, 1978) that the growth rates of ice dendrites are enhanced in dilute solutions. I have proposed a stability mechanism to explain this (Langer, 1978), but the analysis is not yet complete or convincing. In general, the metallurgically important problem of the interplay between thermal and chemical instabilities in solidification seems ripe for new theoretical and experimental investigation.

(5) All of the work on dendrites to date has focused on the behavior of the tip—its velocity, its shape, and the initial sidebranching activity. As can be seen in Fig. 12, the mature sidebranches well behind the tip have coarsened via some kind of selection mechanism; and their ultimate spacing is not the same as the wavelength of the initial disturbance near the tip. It is the coarsened structure which is most interesting met-

allurgically. Can it be predicted? Does the ultimate spacing scale simply like the tip radius as a function of growth parameters, or is there some more complex relationship?

(6) The experimental observations, especially at the smaller undercoolings, indicate an appreciable effect of convective transport in the fluid. How can this effect be accounted for theoretically?

Consider, next, the problems having to do with directional solidification and cellular interfaces. These are the solidification theorist's versions of the Bénard or Taylor instabilities in hydrodynamics. The solidification problems are less thoroughly explored than their hydrodynamic analogs, and there is a notable lack of accurate experimental data—this despite the fact that there exists a rich variety of accessible and technologically interesting phenomena. The most basic questions seem to be the following:

(7) Under what growth conditions do stable, stationary, cellular interfaces occur? A complete differential-stability analysis has been performed only for the somewhat artificial symmetric model and, there, only for the small-amplitude structures which occur when the plane is just weakly unstable. Are larger structures, like that shown in Fig. 19, stable? Are there any stable cellular solutions at all for the more realistic one-sided model? How can one generalize a differential-stability analysis to deal with the possible breakdown of the quasistationary approximation in the latter model? Existing theories deal only with one-dimensional variations of the interfacial displacement. Can the analysis be extended to two-dimensional patterns, for example, hexagonal cells?

(8) What determines the natural periodicity of a restabilized cellular structure? Does there exist a principle of marginal stability which is relevant to this situation?

(9) What happens when the steady-state theory breaks down? How does this breakdown occur? Do the stationary solutions simply disappear? Or do they become unstable while continuing to exist mathematically? What is the role of finite-amplitude—as opposed to differential—instabilities? Are there hysteretic effects?

(10) What sorts of nonstationary solutions occur? Do there exist, for either of the models described in Sec. V, nearly stationary solutions of the kind shown in Fig. 7 where the time-dependent behavior occurs only in the groove roots? Under what conditions does a planar solidification front become dendritic?

(11) Is there an analog, in the solidification problem, of the onset of turbulence in hydrodynamics? That is, are there situations in which the solidification pattern becomes intrinsically chaotic?

The reader will note that, in the last sets of questions, I have ventured away from specific cellular problems and into an area of general principles, and that I am in danger of violating my introductory appeal for detailed spadework. I shall go even further astray in a concluding line of inquiry.

(12) The most interesting pattern-forming processes appear to be intrinsically time dependent. If the marginal-stability hypothesis is valid, they are intrinsically nonlinear. And, if the sidebranching mechanism is characteristic, they are spatially unbounded in a special, controlled sort of way. Is there some generalized notion of stability which is relevant here? As far as I can tell, equations of motion such as (5.2) cannot be recast to look like potential flow. There does not seem to be a simple Liapounov function. Nevertheless, might there be some meaningful and useful variational formulation that describes these processes? What are we missing?

ACKNOWLEDGMENTS

I should like to thank Dr. R. F. Sekerka who has introduced me to most of the areas of research described in this paper. Messrs. K. Kasturi and P. Popper have helped in some of the calculations; and Ms. V. Datye has suggested several important improvements of the manuscript in addition to having done all of the computations leading to Fig. 7. Figure 12 has been reproduced here by courtesy of Dr. M. E. Glicksman. I am particularly grateful to Dr. Glicksman for having provided both photographs and new experimental data prior to publication.

REFERENCES

Abramowitz, M., and I. A. Stegun, 1964, editors, *Handbook of Mathematical Functions* (National Bureau of Standards, Washington, D.C.).
Chalmers, B., 1964, *Principles of Solidification* (Wiley, New York).
Chandrasekhar, S., 1961, *Hydrodynamic and Hydromagnetic Stability* (Oxford University, London).
Delves, R. T., 1975, "Theory of Interface Stability," in *Crystal Growth*, edited by B. R. Pamplin (Pergamon, Oxford).
Doherty, R., 1975, "Dendritic Growth," in *Crystal Growth*, edited by B. R. Pamplin (Pergamon, Oxford).
Fujioka, T., 1978, Ph.D. thesis, Carnegie-Mellon University.
Glansdorff, P., and I. Prigogine, 1971, *Thermodynamics of Structure, Stability, and Fluctuations* (Wiley-Interscience, New York).
Glicksman, M.E., R. J. Shaefer, and J. D. Ayers, 1976, Metall. Trans. A **7**, 1747.
Haken, H., 1977, *Synergetics* (Springer, New York).
Hallett, J., 1964, J. Atmos. Sci. **21**, 671.
Hobbs, P. V., 1974, *Ice Physics* (Clarendon, Oxford).
Holtzman, E. G., 1969, Ph.D. thesis, Stanford University.
Horvay, G., and J. W. Cahn, 1961, Acta Metall. **9**, 695.
Ivantsov, G. P., 1947, Dokl. Akad. Nauk SSSR **58**, 567.
Jackson, K., 1971, "Defect Formation, Microsegregation, and Crystal Growth Morphology," in *Solidification* (American Society for Metals, Metals Park, Ohio).
Jackson, K. A., and J. D. Hunt, 1966, Trans. Met. Soc. of AIME **236**, 1129.
Jackson, K. A., and J. D. Hunt, movie entitled "The Solidification of Single Phase Transparent Materials," Bell Telephone Laboratories Film Library.
Jackson, K. A., D. R. Uhlmann, and J. D. Hunt, 1967, J. Cryst. Growth **1**, 1.
Kallungal, J. P., and A. J. Barduhn, 1977, A.I.Ch.E. J. 294.
Langer, J. S., 1977, Acta Metall. **25**, 1121.
Langer, J. S., and H. Müller-Krumbhaar, 1977, J. Cryst. Growth **42**, 11.
Langer, J. S., and L. A. Turski, 1977, Acta Metall. **25**, 1113.
Langer, J. S., 1978 "Dendritic Solidification of Dilute Solutions," Lecture presented at the Physicochemical Hydrody-

namics Conference, Washington, D. C., to be published in Physicochemical Hydrodynamics.
Langer, J. S., R. F. Sekerka, and T. Fujioka, 1978, J. Cryst. Growth **44**, 414.
Langer, J. S., and H. Müller-Krumbhaar, 1978, Acta Metall. **26**, 1681; 1689; 1697.
Lindenmeyer, C., 1959, Ph.D. thesis, Harvard University.
Lindenmeyer, C. S., and B. Chalmers, 1966, J. Chem. Phys. **45**, 2807.
Macklin, W. C., and B. F. Ryan, 1966, Philos. Mag. **4**, 847.
Macklin, W. C. and B. F. Ryan, 1968, Philos. Mag. **17**, 83.
Morris, L. R., and W. C. Winegard, 1969, J. Cryst. Growth **5**, 361.
Mullins, W. W., and R. F. Sekerka, 1963, J. Appl. Phys. **34**, 323.
Mullins, W. W., and R. F. Sekerka, 1964, J. Appl. Phys. **35**, 444.
Nakaya, U., 1954, *Snow Crystals* (Harvard University, Cambridge, Mass).
Nash, G. E., 1974, Naval Research Laboratory Reports, Nos. 7679 and 7680.
Nash, G. E., and M. E. Glicksman, 1974, Acta Metall. **22**, 1283.
Newell, A. C., and J. A. Whitehead, 1969, J. Fluid Mech. **38**, 279.
Nicolis, G., and I. Prigogine, 1977, *Self-Organization in Non-equilibrium Systems* (Wiley-Interscience, New York).
Oldfield, W., 1973, Mater. Sci. Eng. **11**, 211.
Pruppacher, H. R., 1967, J. Colloid Interface Sci. **25**, 285.
Rubinstein, L. 1971, *The Stefan Problem* (translated by A. D. Solomon (American Mathematical Society, Providence, R. I.).
Müller-Krumbhaar, H., 1978, "Kinetics of Crystal Growth," in *Current Topics in Materials Science*, edited by E. Kaldis (North-Holland, Amsterdam).
Ryan, B. F., 1969, J. Cryst. Growth **5**, 284.
Segel, L. A., 1966, in *Non-Equilibrium Thermodynamics, Variational Techniques and Stability*, edited by R. J. Donnelly, R. Herman, and I. Prigogine (University of Chicago, Chicago).
Sekerka, R. F., R. G. Seidensticker, D. R. Hamilton, and J. D. Harrison, 1967, Investigation of desalination by freezing, Westinghouse Research Laboratory Report, Chap. 3.
Sekerka, R. F., 1967a, J. Phys. Chem. Solids **28**, 983.
Sekerka, R. F., 1967b, in *Crystal Growth*, edited by H. S. Peiser (Pergamon, Oxford), p. 691.
Sekerka, R. F., 1973, "Morphological stability," in *Crystal Growth, an Introduction*, edited by P. Hartman (North-Holland, Amsterdam).
Sekerka, R. F., 1976, in *Physical Chemistry in Metallurgy*, Proceedings of the Darken Conference, U. S. Steel Research Laboratory, p. 311.
Strässler, S., and W. R. Schneider, 1974, Phys. Cond. Matter **17**, 153.
Tarshis, L. A., and W. A. Tiller, 1967, in *Crystal Growth*, edited by H. W. Peiser (Pergamon, Oxford), p. 709.
Temkin, D. E., 1960, Dokl. Akad. Nauk SSSR **132**, 1307.
Thom, R., 1975, *Structural Stability and Morphogenesis* (Benjamin, Reading, Mass.).
Tiller, W. A., K. A. Jackson, J. W. Rutter, and B. Chalmers, 1953, Acta Metall. **1**, 428.
Tiller, W. A., 1961, *Principles of Solidification* (Air Force Office of Scientific Research, Washington, D. C.).
Trivedi, R., 1970, Acta Metall. **18**, 287.
Turnbull, D., 1956, "Phase Changes," in *Solid State Physics*, Vol. 3, edited by F. Seitz and D. Turnbull (Academic, New York), p. 236.
Verhoeven, J. D., and E. D. Gibson, 1972, Metall. Trans. **3**, 1893.
Verhoeven, J. D., and E. D. Gibson, 1973, Metall. Trans. **4**, 2581.
Weeks, J. D., and G. H. Gilmer, 1979, "Dynamics of Crystal Growth," in Adv. Chem. Phys. **40** (to be published).
Whitehead, J. A. Jr., 1975, "A survey of hydrodynamic instabilities," in *Fluctuations, Instabilities, and Phase Transitions*, edited by T. Riste (Plenum, New York).
Wollkind, D., and L. Segel, 1970, Phil. Trans. R. Soc. (Lond.) **268**, 351.

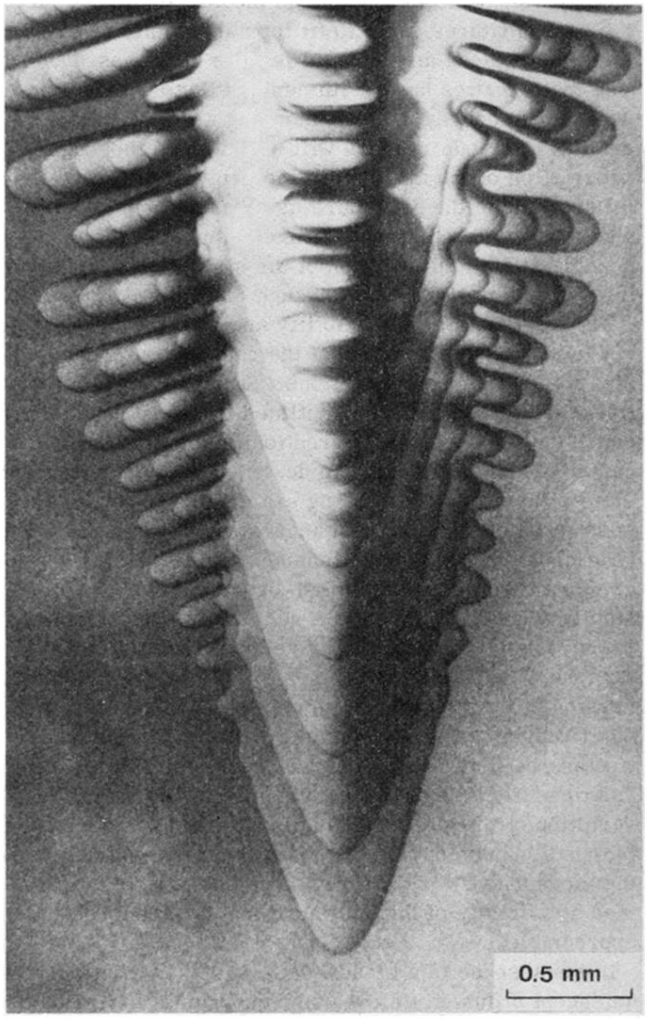

FIG. 12. Multiple-exposure photograph of a downward-growing succinonitrile dendrite (Glicksman, to be published).

FIG. 3. Photograph of dendritic ice crystal grown in pure water at an undercooling of $T_M - T = 2.34°C$ (Fujioka, 1978).